Molybdenum isotope evidence for extensive crustal extraction and recycling in Earth's first billion years

Alex J. McCoy-West[1, 2], Priyadarshi Chowdhury[2], Kevin W. Burton[1], Paolo Sossi[3], Geoff M. Nowell[1], J. Godfrey Fitton[4], Andrew C. Kerr[5], Peter A. Cawood[2] and Helen M. Williams[1,6]

[1]Department of Earth Sciences, Durham University, Elvet Hill, Durham DH1 3LE, UK

[2]School of Earth, Atmosphere and Environment, Monash University, Clayton, Victoria, 3800, Australia

[3]Institute of Geochemistry and Petrology, ETH Zürich

[4]School of GeoSciences, University of Edinburgh, Edinburgh EH9 3FE, UK

[5]School of Earth and Ocean Sciences, Cardiff University, Park Place, Cardiff CF10 3AT, UK

[6]Department of Earth Sciences, University of Cambridge, Downing Street, Cambridge CB2 3EQ, UK

Number of words:	3,029
Number of references:	49
Number of figures:	4
First paragraph (words):	151
Caption Length (words):	100, 96, 64, 90
Methods number of words:	1,190

Corresponding Author

Alex McCoy-West (alex.mccoywest@monash.edu)

School of Earth, Atmosphere and Environment, Monash University, Clayton, Victoria, 3800, Australia

FIRST PARAGRAPH

Estimates of the volume of the earliest crust based on zircon ages and radiogenic isotopes remain equivocal. Stable isotope systems, such as molybdenum (Mo), have the potential to provide further constraints but remain underused, due to the lack of complementarity between mantle and crustal reservoirs. We present Mo isotope data for Archean komatiites and Phanerozoic komatiites and picrites and demonstrate that their mantle sources all possess sub-chondritic signatures complementary to the super-chondritic continental crust. These results confirm that the present-day degree of mantle depletion was achieved by 3.5 billion years ago and that the Earth has been in a steady state with respect to Mo recycling. Mass balance modelling shows that this early mantle depletion requires the extraction of a far greater volume of mafic-dominated proto-crust than previous thought, more than twice the volume of the continental crust today, implying rapid crustal growth and destruction of crust in the first billion years of Earth's history.

MAIN TEXT

The nature, extent and geodynamic settings of crustal formation and recycling are poorly constrained, particularly during Hadean-early Archean times for which the rock-record is scarce[1,2]. The growth of the crust is estimated to be either temporally skewed with >60-80% of the present-day volume of continental crust (PVCC) forming by 3 billion years ago (Ga)[2-5], or much more gradual with time[1,6]. These growth curves are derived either from zircon formation ages[1,2] or from radiogenic isotopic evolution within the crust-mantle system[6-8]. Zircon ages provide the lower bound on crustal growth as they cannot constrain the magnitude of recycling. In contrast, growth curves of radiogenic isotope systems track the evolution of mantle depletion and implicitly consider both crust extraction and recycling[3,9]. The complementarity of the crustal and mantle reservoirs for long-lived radiogenic isotopes (Sr-Nd-Hf) has long been established, with time-dependent models requiring that only ~25-50% of the mantle's mass underwent melt extraction to balance the present-day compositions of the depleted mantle and crust[7,8,10]. Estimating crustal growth from a mantle-depletion perspective using time-invariant proxies provides an alternative approach[4]. The ratios of stable isotopes being independent of time, fit this criterion and can put quantitative constraints on differentiation processes occurring in the early Earth. However, this approach is hindered by the lack of resolvable isotopic variation in samples representative of the depleted mantle and crust for many non-traditional stable isotope systems.

Molybdenum stable isotopes ($\delta^{98}Mo = [(^{98}Mo/^{95}Mo_{sample} / {}^{98}Mo/^{95}Mo_{standard}) - 1] \times 1000$; with the standard NIST3134 = 0‰) may be an exception, with a picture emerging of two complementary reservoirs in the crust and mantle. Chondritic meteorites, the purported building blocks of the terrestrial planets, have a relatively homogeneous average $\delta^{98}Mo$ of -0.154 ± 0.013‰[11,12] (all errors on averages herein are 95% standard errors). Estimates of the

composition of the modern continental crust based on molybdenites, granites and primitive arc-related basalts yield super-chondritic δ^{98}Mo values ranging from +0.05‰ to +0.3‰[13-15]. If the bulk Earth is chondritic with respect to Mo stable isotopes and Mo is not fractionated during its partitioning into Earth's core (cf. [16]), then an isotopically light, sub-chondritic Mo reservoir must exist in the mantle[17,18]. Arc lavas show extremely variable δ^{98}Mo (−0.88‰ to +0.24‰) but the consensus is that subduction zones appear to be fluxing isotopically light Mo into the mantle[19-21]. However, whether this material is efficiently recycled or has enough mass to affect the composition of the bulk mantle remains to be established. Previous Mo isotope analyses of Archean komatiites[17] have slightly sub-chondritic compositions, but within error of chondrites[11], while five of the most depleted (^{143}Nd/^{144}Nd >0.5131) mid-ocean ridge basalts (MORB) measured are resolvably sub-chondritic[22]. Therefore, it is possible that a complementary light sub-chondritic Mo isotope reservoir is present within the mantle[18], but its composition and nature remains poorly constrained.

Here, we focus on komatiite and picrite samples from four well characterized suites: two from the Archean, the 3.5 Ga Komati (South Africa) and 2.7 Ga Munro (Canada) komatiites[23], and two from the Phanerozoic, the 89 Ma Gorgona (Colombia) komatiites[24] and the 61 Ma Baffin Island (NE Canada) picrites[25,26], to better constrain the Mo isotope composition of the mantle throughout Earth's history. The selection of rock samples for this purpose is non-trivial due to the complex behaviour of Mo during mantle melting. None of the major mineral phases in the mantle host significant Mo[27], and the presence of residual sulfides will strongly affect the Mo concentration of a melt owing given its chalcophile nature[18]. Furthermore, isotopic studies of Mo isotopes in ultramafic lithologies are hampered by the low concentration of Mo (<50 ng/g) and the significant isotopic variability in mantle lithologies[12,17]. Our studied ultramafic lavas formed at elevated temperatures (>1400 °C) by high-degrees of partial melting (>25%), which would have lead to complete sulfide extraction

63 from their source regions[28], such that their Mo isotope compositions closely resemble that of
64 their mantle source regions. Our new results combined with the existing data are used to
65 constrain the δ^{98}Mo of the Earth's mantle, and subsequently global crustal volumes, during
66 Hadean-Archean times.

67

68 **ESTABLISHING A SUB-CHONDRITIC MO ISOTOPE RESERVIOR**

69 Our measurements show sub-chondritic values for unaltered Archean Komati and Munro
70 komatiites with δ^{98}Mo varying from −0.22 to −0.18‰ (Fig. 1; Table S1). Previous analyses
71 of Archean komatiites presented in Greber et al.[17] define a wide range (−0.32‰ < δ^{98}Mo <
72 +0.07‰) with an average δ^{98}Mo of the four investigated localities calculated as −0.210
73 ±0.098‰. Combing these results is not straightforward. For example, previously analysed
74 samples from the Vetreny Belt, Fennoscandia have experienced significant crustal
75 assimilation[29] and consequently display resolvably heavier δ^{98}Mo (−0.077 ±0.083‰). We
76 thus disregard these samples in subsequent interpretations. In Greber et al.[17], lavas from the
77 Komati Formation that were undoubtedly modified by alteration were excluded (Fig. 1;
78 δ^{98}Mo up to +0.44‰), but no further filtering for alteration was attempted. Given the high
79 mobility of Mo in fluids at low temperatures[30], we have filtered the Archean komatiite Mo
80 isotope data (Fig. S1), excluding samples that display major element mobility unrelated to
81 magmatic differentiation and are thus considered to have been modified by alteration (see
82 supplement). Our new data, along with the alteration-filtered dataset of [17], allows the
83 calculation of the δ^{98}Mo of Archean komatiites as −0.199 ±0.019‰.

84 Samples from the Phanerozoic Gorgona komatiites, the freshest komatiite occurrence
85 in the world, have a restricted range of δ^{98}Mo from −0.18 to −0.25‰ and yield an average
86 δ^{98}Mo of −0.207 ±0.034‰, which is within error of their Archean equivalents. In contrast,

87 the Phanerozoic Baffin Island picrites possess variable δ^{98}Mo from −0.13 to −0.32‰, which
88 at first glance suggests a lighter composition (Fig. 1). However, the Baffin Island picrites
89 represent a special case of disequilibrium olivine accumulation[26] and after correction the
90 composition of the parental melt is calculated as δ^{98}Mo = −0.210 ±0.010‰ (Table S2). The
91 δ^{98}Mo of the Baffin Island parental melts are thus within error of depleted MORB[22], the
92 Gorgona komatiites, and three Archean komatiite localities that span 800 Ma, suggesting that
93 the Mo isotope composition of the accessible mantle has changed little over the last 3.5 Ga.
94 These data for magmatic rocks are augmented by mantle xenoliths to calculate the average
95 composition of the depleted mantle as δ^{98}Mo = −0.204 ±0.008‰ (Table S3).

96 These results place several new constraints on the evolution of Earth's mantle,
97 notably: 1) the Mo isotope composition of the accessible mantle is unambiguously sub-
98 chondritic (an analysis of variance test confirms that the mantle samples are a resolvably
99 different population to chondritic meteorites at the 99% significance level; p-value <0.001);
100 2) the formation of this reservoir must have occurred before ~3.5 Ga, 3) it must have had a
101 substantial volume (magmas generated at a range of melting depths are affected); and 4) no
102 resolvable temporal variations are observed with Archean komatiites ranging in age from
103 3.5−2.7 Ga having identical δ^{98}Mo to Cretaceous Gorgona komatiites and Paleogene Baffin
104 Island picrites and modern MORB (an analysis of variance test confirms that the means of
105 these populations are identical; p-value ~0.42). Together these constraints demonstrate that
106 most of the present-day depletion of the mantle must have been completed by the
107 Paleoarchean. This finding is in agreement with independent constraints on the temporal
108 chemical evolution of continental basalts, which indicates a nearly constant amount of mantle
109 depletion since ~3.8 Ga[31]. However, the amount of mantle depletion, and hence the volume
110 of early continental crust produced and subsequently destroyed, remain under-constrained[3,9].
111 Nonetheless, most studies agree that 30−50% melt depletion of the whole mantle can

reproduce most of the radiogenic and incompatible element signatures of the crust and depleted mantle, assuming they represent complementary reservoirs[7,8,10]. This has significant implications for the growth of early crust given that the proto-crust and depleted mantle should chemically complement each other, if no other processes have perturbed the system. We explore this further below.

COMPOSITION OF THE SILICATE EARTH

Due to the refractory nature of Mo in the solar nebula, we assume that the proto-Earth inherited the δ^{98}Mo of chondritic meteorites (Fig. 2). Soon after accretion, core formation occurred (≈ 34 Ma[32]) resulting in the efficient removal of the highly siderophile elements into the Fe-Ni metal core, including 95% of the Earth's original Mo[33] (Table S5). The near quantitative removal of Mo to the core means isotope ratios in the metallic phase are unlikely to be fractionated from those in bulk chondrites, as observed in iron meteorites[11]. Early experimental work suggested this sequestration of Mo may have been associated with a small but resolvable isotopic fractionation of the silicate portion of the planet[34]. However, recent metal-silicate experiments which incorporate the effect of Mo valence state[16] suggest a significantly reduced $\Delta^{98}Mo_{metal\text{-}silicate}$ of as little as −0.008‰ (assuming $Mo^{6+}/\sum Mo = 0.1$; T = 2500 °C), which means the mantle would remain within the error of the composition of chondrites following core formation. Subsequent modification of the residual bulk silicate Earth (BSE) may have occurred during: 1) the Moon-forming impact: where an planet-sized body impacted Earth and added volatiles, including significant sulfur, which were then sequestered to the outer core in the "Hadean matte" (<1% of core mass; this sulfide-enriched phase is expected to have preferentially incorporated isotopically light Mo[35,36]); or 2) late accretion: since geochemical modelling suggests that all of the Mo in Earth's mantle was added during the last 10% of accretion[37], with *N*-body simulations require only ~1% of the

Earth's mass was accreted following the Moon-forming impact[38]. Ultimately, due to the chondritic composition of the new materials these processes will not significantly change the δ^{98}Mo of the BSE, which should be around δ^{98}Mo ≈ −0.154 ‰. Therefore, the only remaining global-scale mechanism that can modify the Earth's Mo isotope budget and account for the Earth's super-chondritic crust and sub-chondritic mantle is the extraction of the crust (Fig. 2). Furthermore, the presence of positive Nb anomalies and radiogenic Nd isotope compositions in some komatiite suites suggest that their source regions have previously undergone melt extraction[23].

EXTRACTION OF AN ISOTOPICALLY HEAVY CRUST

The sub-chondritic mantle δ^{98}Mo signature may be the result of partial melting[22] or continental crust extraction[17] or both, but the exact magnitude of fractionation remains uncertain. Here we have developed a partial melting model to assess the direction and magnitude of fractionation of δ^{98}Mo between melt and residual mantle (Fig. 3). This modelling demonstrates several important points: 1) high-MgO partial melts are accurate recorders of the Mo isotope composition of their mantle sources because at high temperatures $\Delta^{98}Mo_{melt\text{-}solid}$ <0.012‰ at 30% melting (Fig. 3a); 2) melting of a chondritic reservoir to form basalt reproduces the average basalt used in modelling (δ^{98}Mo = −0.10 ‰) with ~12% melting at 1300 °C. This ~0.05‰ difference in δ^{98}Mo is comparable to that observed between N-MORB[22] and the depleted mantle composition (herein); 3) the composition of modern upper continental crust or Phanerozoic granites (Fig. 1; $\Delta^{98}Mo_{granite\text{-}mantle}$ +0.36‰) cannot be generated by direct melting of the mantle. The majority of the enrichment of these samples in heavy δ^{98}Mo must instead result from intracrustal differentiation, either through the addition of isotopically heavy subduction zone fluids[19] or hydrothermal fluids[39] or the removal of isotopically light hydrous phases (biotite or amphibole)[13] into cumulates in the lower crust.

Molybdenum isotope fractionation during melt extraction may be driven by both changes in Mo oxidation state and co-ordination number. Given that Mo^{6+} is significantly more incompatible than Mo^{4+}[27] residues of melting will have lower $Mo^{6+}/\sum Mo$ than melt in addition to higher mean co-ordination number, and hence will display lighter $\delta^{98}Mo$ consistent with sense of fractionation observed in the komatiites measured herein (Fig. 1). The oxidation state of Mo in the modern mantle remains uncertain, however, partitioning studies indicate Mo is predominantly hexavalent in melts at typical upper mantle conditions ($Mo^{6+}/\sum Mo \approx 0.99$[16,27,40]). Although mantle oxygen fugacity is generally considered to have been constant for the last ~3.5 Ga[41], recent work using V partitioning provides strong evidence of increasing oxygen fugacity with time[42], therefore here we impose $Mo^{6+}/\sum Mo$ = 0.95 for early mantle melting (Fig. 3b). Creation of felsic components of the Hadean-Eoarchean crust such as tonalite-trondhjemite-granodiorite (TTG) granitoids, requires remelting of metabasalt (mafic amphibolite)[43], which will further enrich this felsic component in heavier isotopes by up to 0.08‰ (at 900 °C and F = 20%), but cannot explain the full range of heavy $\delta^{98}Mo$ observed. The models presented here evaluate mantle melting only and should be considered minimum estimates and approximate until Mo isotope fractionation factors can be independently determined for accessory phases that may retain isotopically light Mo (e.g. garnet, amphibole, sulfide). Nonetheless, they demonstrate that there is no need to invoke subduction zone processes in the early Earth to form the mafic crusts discussed below, which can instead be generated solely through mantle melting processes.

EXTENSIVE EXTRACTION AND RECYCLING OF EARLY CRUST

Assuming a two-reservoir model involving a proto-crust(C) and depleted mantle(DM), we have estimated the crustal volume that is required to have formed by ~3.5 Ga to reconcile the

183 δ^{98}Mo and Mo-concentration of the mantle that sourced the Archean komatiites using the
184 mass-balance equation:

$$m_C = \frac{m_{DM} \,.\, [Mo]_{DM} \,.\, (\delta^{98}_{BSE} - \delta^{98}_{DM})}{[Mo]_C \,.\, (\delta^{98}_{C} - \delta^{98}_{BSE})}$$

185 where m_i , $[Mo]_i$ and δ_i^{98} represents the mass, Mo concentration and Mo isotope
186 composition, respectively, of the various reservoirs. It is important to note the mass balance
187 modelling presented here does not reflect the instantaneous removal of melts from the mantle,
188 but rather the effect of the time-integrated isolation of the proto-crust from the convecting
189 mantle.

190 Calculations of continental growth based on the zircon archive and mantle depletion
191 commonly use the present-day continental crust as the crustal endmember. However, there
192 are two major compositional differences between the early continents and their modern
193 analogues[2,8] . These are: 1) TTG granitoids were the dominant felsic rocks with true potassic
194 (K) granites subordinate in abundance[43] and, 2) mafic lithologies were more abundant than
195 their felsic counterparts[44,45]. Here we assume the BSE had an initial δ^{98}Mo equal to chondritic
196 meteorites (for alternate scenarios Fig. S6) and have investigated two scenarios to encompass
197 the variability of δ^{98}Mo in Archean felsic rocks (granites or TTGs represent the felsic
198 endmember; Fig. 4). These scenarios thus provide the minimum and maximum estimates of
199 the extent of pre-3.5 Ga crust extraction. We have then calculated crustal volumes for three
200 different model proto-crusts: a hypothetical purely felsic crust, Mafic crust-A (minimum
201 based on a mafic crust) and Mafic crust-B (a likely Eoarchean crustal composition).
202 Calculations based on the purely felsic crusts suggest a minimum of 0.5-1.5 times the PVCC
203 (~7.2x10^9 km^3) existed prior to 3.5 Ga based on 30 % depletion of the whole mantle (Fig. 4).
204 This range is consistent with the growth model calculated using Nb/U ratios of the crust-

mantle system[4], but is higher than those calculated using the crustal zircon formation ages (<50% of PVCC at 3.5 Ga;[2]). This suggests that time-invariant proxies of mantle depletion record similar volumes of early crust extraction, whereas their difference with the zircon-based models reflects the influence of crustal recycling. More realistic calculations based on dominantly mafic crust types require crustal volumes greater than the PVCC by ~3.5 Ga (Fig 4). For example, in the preferred Eoarchean scenario with a TTG felsic component the crustal volumes based on Mafic crust-A and –B will be 2.5 and 3.8 times the PVCC, respectively, assuming the minimum likely amount of mantle depletion (30%; [7,8,10]; Fig. 4b). These higher values are mostly a consequence of the lower Mo concentration (and to a minor extent the lighter isotopic compositions) of these model crusts (see Table S5). It is debatable whether to consider dominantly mafic crust as continental or not[44,45], but our calculations show that even the volume of a hypothetical TTG crust would have been greater than the PVCC, provided the depleted mantle size exceeds ~20% of the whole mantle. Thus, it is highly likely that a greater volume of crust than the PVCC was extracted in the first billion years of Earth's history, most of which was then subsequently recycled into the mantle.

Large-scale crust extraction is consistent with the prediction of voluminous melting of the mantle owing to its hotter thermal structure during Hadean-Archean times[46]. However, our calculated crustal volumes represent the amount of crust extracted from the mantle and not its net growth, which is determined by the difference between extracted (generated) and recycled volumes of the crust[9]. Nevertheless, high rates of crust formation should result in rapid crustal growth unless the recycling rates equal or exceed extraction rates. Several independent continental growth models[2,3,5] do suggest extremely rapid continental growth consistent with the idea that extensive crust formation may have happened on the early Earth. Given the dearth of such old rocks in the present rock record, it is unequivocal that much of the >3.5 Ga crust has been recycled. Mantle-derived isotopic heterogeneities are widespread

in modern basalts, reflecting sluggish mantle mixing. Modelling of stagnant lid regimes shows that mixing was up to an order of magnitude slower under these conditions[47] therefore it is expected that this recycled crustal material will not have mixed back completely into the accessible mantle. Although difficult to constrain, recent studies on Archean continental recycling[48,49] suggest extensive recycling (but not exceeding the formation rates) of the crust, with a volume equivalent to the PVCC probably recycled during the late Archean[48]. If the recycling rates were similar during most of the Hadean-Archean, twice the PVCC could have been recycled back into the mantle during that period. Consequently, we have not only been significantly underestimating the volumes of early formed crust, but also the amount of material that was being recycled back into the mantle.

Acknowledgements

Dave Selby is thanked for access to carius tube facilities. This project was funded by a European Research Council Starting Grant ("HabitablePlanet" 306655) to HMW and a NERC Grant (NE/M0003/1) to KWB. While at Monash AMW, PC and PAC were supported by ARC grant FL160100168.

Author Contributions

AMW and HMW conceived the study. AMW undertook the chemistry and mass spectrometry with assistance from GMN. JGF, ACK and PS provided the samples. AMW and PC developed the mass balance modelling. AMW and PS developed the Mo isotope partial melting model. All authors contributed to discussions on early crustal volumes and writing and editing the paper.

REFERENCES

1 Condie, K. C. Episodic continental growth and supercontinents: a mantle avalanche connection? *Earth and Planetary Science Letters* **163**, 97-108 (1998).

2 Dhuime, B., Hawkesworth, C. J., Cawood, P. A. & Storey, C. D. A change in the geodynamics of continental growth 3 billion years ago. *Science* **335**, 1334-1336, doi:10.1126/science.1216066 (2012).

3 Korenaga, J. Estimating the formation age distribution of continental crust by unmixing zircon ages. *Earth and Planetary Science Letters* **482**, 388-395, doi:https://doi.org/10.1016/j.epsl.2017.11.039 (2018).

4 Campbell, I. H. Constraints on continental growth models from Nb/U ratios in the 3.5 Ga Barberton and other Archaean basalt-komatiite suites. *American Journal of Science* **303**, 319-351, doi:10.2475/ajs.303.4.319 (2003).

5 Armstrong, R. L. Radiogenic isotopes: the case for crustal recycling on a near-steady-state no-continental-growth Earth. *Philosophical Transactions of the Royal Society of London* **301**, 443-472, doi:10.1098/rsta.1981.0122 (1981).

6 McCulloch, M. T. & Bennett, V. C. Progressive growth of the Earth's continental crust and depleted mantle: Geochemical constraints. *Geochimica et Cosmochimica Acta* **58**, 4717-4738, doi:http://dx.doi.org/10.1016/0016-7037(94)90203-8 (1994).

7 DePaolo, D. J. Crustal growth and mantle evolution: inferences from models of element transport and Nd and Sr isotopes. *Geochimica et Cosmochimica Acta* **44**, 1185-1196, doi:https://doi.org/10.1016/0016-7037(80)90072-1 (1980).

8 Jacobsen, S. B. Isotopic and chemical constraints on mantle-crust evolution. *Geochimica et Cosmochimica Acta* **52**, 1341-1350, doi:https://doi.org/10.1016/0016-7037(88)90205-0 (1988).

9 Cawood, P. A., Hawkesworth, C. J. & Dhuime, B. The continental record and the generation of continental crust. *GSA Bulletin* **125**, 14-32, doi:10.1130/B30722.1 (2013).

10 O'Nions, R. K., Evensen, N. M. & Hamilton, P. J. Geochemical modeling of mantle differentiation and crustal growth. *Journal of Geophysical Research: Solid Earth* **84**, 6091-6101, doi:doi:10.1029/JB084iB11p06091 (1979).

11 Burkhardt, C., Hin, R. C., Kleine, T. & Bourdon, B. Evidence for Mo isotope fractionation in the solar nebula and during planetary differentiation. *Earth and Planetary Science Letters* **391**, 201-211, doi:http://dx.doi.org/10.1016/j.epsl.2014.01.037 (2014).

12 Liang, Y.-H. *et al.* Molybdenum isotope fractionation in the mantle. *Geochimica et Cosmochimica Acta* **199**, 91-111, doi:https://doi.org/10.1016/j.gca.2016.11.023 (2017).

13 Voegelin, A. R., Pettke, T., Greber, N. D., von Niederhäusern, B. & Nägler, T. F. Magma differentiation fractionates Mo isotope ratios: Evidence from the Kos Plateau Tuff (Aegean Arc). *Lithos* **190–191**, 440-448, doi:http://dx.doi.org/10.1016/j.lithos.2013.12.016 (2014).

14 Yang, J. *et al.* The molybdenum isotopic compositions of I-, S- and A-type granitic suites. *Geochimica et Cosmochimica Acta* **205**, 168-186, doi:https://doi.org/10.1016/j.gca.2017.01.027 (2017).

15 Greber, N. D., Pettke, T. & Nägler, T. F. Magmatic–hydrothermal molybdenum isotope fractionation and its relevance to the igneous crustal signature. *Lithos* **190-191**, 104-110, doi:https://doi.org/10.1016/j.lithos.2013.11.006 (2014).

16 Hin, R. C., Burnham, A. D., Gianolio, D., Walter, M. J. & Elliott, T. Molybdenum isotope fractionation between Mo4+ and Mo6+ in silicate liquid and metallic Mo. *Chemical Geology* **504**, 177-189, doi:https://doi.org/10.1016/j.chemgeo.2018.11.014 (2019).

17 Greber, N. D., Puchtel, I. S., Nägler, T. F. & Mezger, K. Komatiites constrain molybdenum isotope composition of the Earth's mantle. *Earth and Planetary Science Letters* **421**, 129-138, doi:https://doi.org/10.1016/j.epsl.2015.03.051 (2015).

18 Willbold, M. & Elliott, T. Molybdenum isotope variations in magmatic rocks. *Chemical Geology* **449**, 253-268, doi:https://doi.org/10.1016/j.chemgeo.2016.12.011 (2017).

19 Freymuth, H., Vils, F., Willbold, M., Taylor, R. N. & Elliott, T. Molybdenum mobility and isotopic fractionation during subduction at the Mariana arc. *Earth and Planetary Science Letters* **432**, 176-186, doi:http://dx.doi.org/10.1016/j.epsl.2015.10.006 (2015).

20 Gaschnig, R. M. *et al.* The Molybdenum Isotope System as a Tracer of Slab Input in Subduction Zones: An Example From Martinique, Lesser Antilles Arc. *Geochemistry, Geophysics, Geosystems* **18**, 4674-4689, doi:doi:10.1002/2017GC007085 (2017).

21 König, S., Wille, M., Voegelin, A. & Schoenberg, R. Molybdenum isotope systematics in subduction zones. *Earth and Planetary Science Letters* **447**, 95-102, doi:https://doi.org/10.1016/j.epsl.2016.04.033 (2016).

22 Bezard, R., Fischer-Gödde, M., Hamelin, C., Brennecka, G. A. & Kleine, T. The effects of magmatic processes and crustal recycling on the molybdenum stable isotopic composition of Mid-Ocean Ridge

Basalts. *Earth and Planetary Science Letters* **453**, 171-181, doi:http://dx.doi.org/10.1016/j.epsl.2016.07.056 (2016).
23 Sossi, P. A. *et al.* Petrogenesis and Geochemistry of Archean Komatiites. *Journal of Petrology* **57**, 147-184, doi:10.1093/petrology/egw004 (2016).
24 Kerr, A. C. *et al.* The petrogenesis of Gorgona komatiites, picrites and basalts: new field, petrographic and geochemical constraints. *Lithos* **37**, 245-260, doi:http://dx.doi.org/10.1016/0024-4937(95)00039-9 (1996).
25 Starkey, N. A. *et al.* Helium isotopes in early Iceland plume picrites: Constraints on the composition of high 3He/4He mantle. *Earth and Planetary Science Letters* **277**, 91-100, doi:https://doi.org/10.1016/j.epsl.2008.10.007 (2009).
26 McCoy-West, A. J., Godfrey Fitton, J., Pons, M.-L., Inglis, E. C. & Williams, H. M. The Fe and Zn isotope composition of deep mantle source regions: Insights from Baffin Island picrites. *Geochimica et Cosmochimica Acta* **238**, 542-562, doi:https://doi.org/10.1016/j.gca.2018.07.021 (2018).
27 Leitzke, F. P. *et al.* Redox dependent behaviour of molybdenum during magmatic processes in the terrestrial and lunar mantle: Implications for the Mo/W of the bulk silicate Moon. *Earth and Planetary Science Letters* **474**, 503-515, doi:https://doi.org/10.1016/j.epsl.2017.07.009 (2017).
28 McCoy-West, A. J., Bennett, V. C., O'Neill, H. S. C., Hermann, J. & Puchtel, I. S. The interplay between melting, refertilization and carbonatite metasomatism in off-cratonic lithospheric mantle under Zealandia: An integrated major, trace and platinum group element study. *Journal of Petrology* **56**, 563-604, doi:10.1093/petrology/egv011 (2015).
29 Puchtel, I. S. *et al.* Petrology of a 2.41 Ga remarkably fresh komatiitic basalt lava lake in Lion Hills, central Vetreny Belt, Baltic Shield. *Contributions to Mineralogy and Petrology* **124**, 273-290, doi:10.1007/s004100050191 (1996).
30 Keppler, H. & Wyllie, P. J. Partitioning of Cu, Sn, Mo, W, U, and Th between melt and aqueous fluid in the systems haplogranite-H2O−HCl and haplogranite-H2O−HF. *Contributions to Mineralogy and Petrology* **109**, 139-150, doi:10.1007/bf00306474 (1991).
31 Keller, B. & Schoene, B. Plate tectonics and continental basaltic geochemistry throughout Earth history. *Earth and Planetary Science Letters* **481**, 290-304, doi:https://doi.org/10.1016/j.epsl.2017.10.031 (2018).
32 Kleine, T. & Walker, R. J. Tungsten Isotopes in Planets. *Annual Review of Earth and Planetary Sciences* **45**, 389-417, doi:10.1146/annurev-earth-063016-020037 (2017).
33 McDonough, W. F. in *Treatise on Geochemistry (First Edition)* Vol. 2 (eds Heinrich D. Holland & Karl K. Turekian) 547-568 (Elsevier, 2003).
34 Hin, R. C., Burkhardt, C., Schmidt, M. W., Bourdon, B. & Kleine, T. Experimental evidence for Mo isotope fractionation between metal and silicate liquids. *Earth and Planetary Science Letters* **379**, 38-48, doi:http://dx.doi.org/10.1016/j.epsl.2013.08.003 (2013).
35 Savage, P. S. *et al.* Copper isotope evidence for large-scale sulphide fractionation during Earth's differentiation. *Geochemical Perspectives Letters* **1**, 53-64, doi:http://dx.doi.org/10.7185/geochemlet.1506 (2015).
36 McCoy-West, A. J., Millet, M.-A. & Burton, K. W. The neodymium stable isotope composition of the silicate Earth and chondrites. *Earth and Planetary Science Letters* **480**, 121-132, doi:https://doi.org/10.1016/j.epsl.2017.10.004 (2017).
37 Dauphas, N. The isotopic nature of the Earth's accreting material through time. *Nature* **541**, 521, doi:10.1038/nature20830
https://www.nature.com/articles/nature20830#supplementary-information (2017).
38 Jacobson, S. A. *et al.* Highly siderophile elements in Earth's mantle as a clock for the Moon-forming impact. *Nature* **508**, 84, doi:10.1038/nature13172 (2014).
39 Neely, R. A. *et al.* Molybdenum isotope behaviour in groundwaters and terrestrial hydrothermal systems, Iceland. *Earth and Planetary Science Letters* **486**, 108-118, doi:https://doi.org/10.1016/j.epsl.2017.11.053 (2018).
40 O'Neill, H. S. C. & Eggins, S. M. The effect of melt composition on trace element partitioning: an experimental investigation of the activity coefficients of FeO, NiO, CoO, MoO2 and MoO3 in silicate melts. *Chemical Geology* **186**, 151-181, doi:http://dx.doi.org/10.1016/S0009-2541(01)00414-4 (2002).
41 Hibbert, K. E. J., Williams, H. M., Kerr, A. C. & Puchtel, I. S. Iron isotopes in ancient and modern komatiites: Evidence in support of an oxidised mantle from Archean to present. *Earth and Planetary Science Letters* **321–322**, 198-207, doi:http://dx.doi.org/10.1016/j.epsl.2012.01.011 (2012).
42 Nicklas, R. W. *et al.* Secular mantle oxidation across the Archean-Proterozoic boundary: Evidence from V partitioning in komatiites and picrites. *Geochimica et Cosmochimica Acta* **250**, 49-75, doi:https://doi.org/10.1016/j.gca.2019.01.037 (2019).

43 Moyen, J.-F. & Laurent, O. Archaean tectonic systems: A view from igneous rocks. *Lithos* **302-303**, 99-125, doi:https://doi.org/10.1016/j.lithos.2017.11.038 (2018).
44 Dhuime, B., Wuestefeld, A. & Hawkesworth, C. J. Emergence of modern continental crust about 3 billion years ago. *Nature Geoscience* **8**, 552, doi:10.1038/ngeo2466 https://www.nature.com/articles/ngeo2466#supplementary-information (2015).
45 Tang, M., Chen, K. & Rudnick, R. L. Archean upper crust transition from mafic to felsic marks the onset of plate tectonics. *Science* **351**, 372-375, doi:10.1126/science.aad5513 (2016).
46 Herzberg, C., Condie, K. & Korenaga, J. Thermal history of the Earth and its petrological expression. *Earth and Planetary Science Letters* **292**, 79-88, doi:https://doi.org/10.1016/j.epsl.2010.01.022 (2010).
47 O'Neill, C., Debaille, V. & Griffin, W. Deep earth recycling in the Hadean and constraints on surface tectonics. *American Journal of Science* **313**, 912-932, doi:10.2475/09.2013.04 (2013).
48 Chowdhury, P., Gerya, T. & Chakraborty, S. Emergence of silicic continents as the lower crust peels off on a hot plate-tectonic Earth. *Nature Geoscience* **10**, 698, doi:10.1038/ngeo3010 https://www.nature.com/articles/ngeo3010#supplementary-information (2017).
49 Johnson, T. E., Brown, M., Kaus, B. J. P. & VanTongeren, J. A. Delamination and recycling of Archaean crust caused by gravitational instabilities. *Nature Geoscience* **7**, 47, doi:10.1038/ngeo2019 https://www.nature.com/articles/ngeo2019#supplementary-information (2013).

Figures

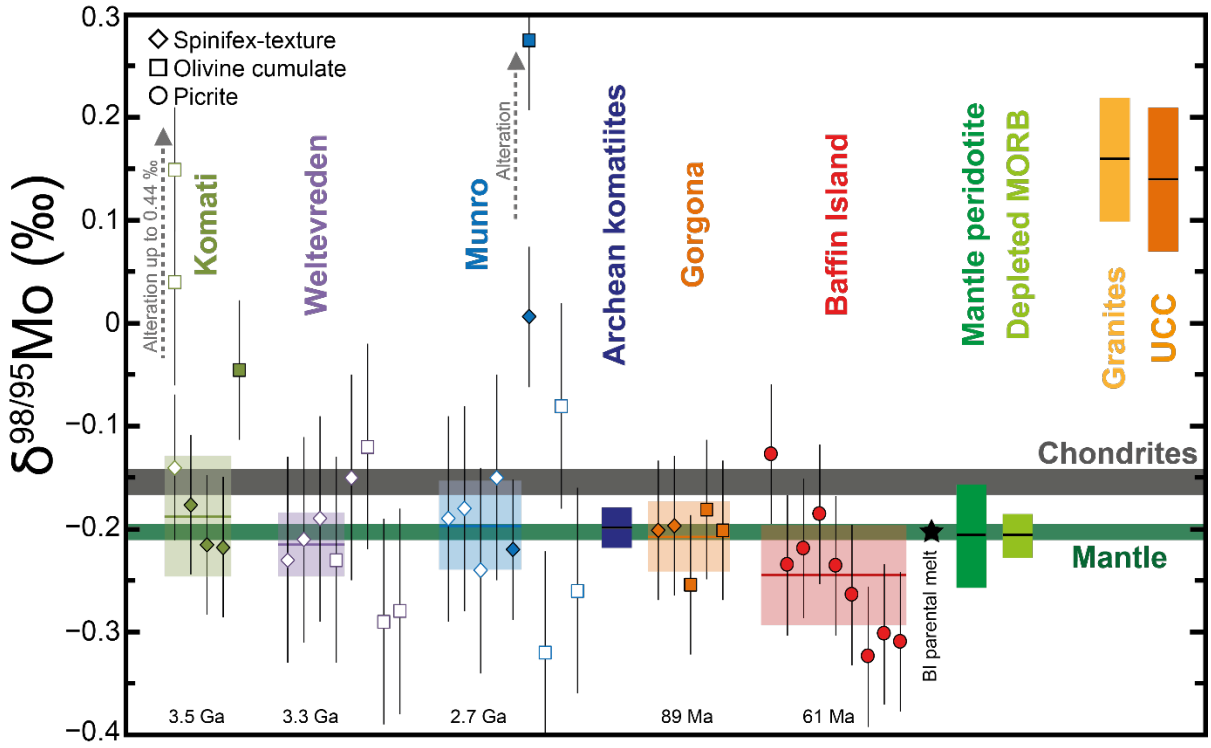

Figure 1: Variation of δ^{98}Mo in komatiites, picrites and major mantle and crustal reservoirs. Filled symbols are data analysed herein with hollow symbols data taken from Greber et al. [17]. All individual analyses are plotted with the 2 standard deviation long term error, with the shaded areas for different formations and reservoirs the being 95% standard errors. The dark grey band represents chondritic meteorites (δ^{98}Mo = −0.154 ±0.013‰; [11,12]) with the green bar representing the resolvable lighter depleted mantle (δ^{98}Mo = −0.204 ±0.008‰; herein). Average Archean komatiites (δ^{98}Mo = −0.199 ±0.019‰; herein) with other reservoirs from [12,14,22] (see Table S3).

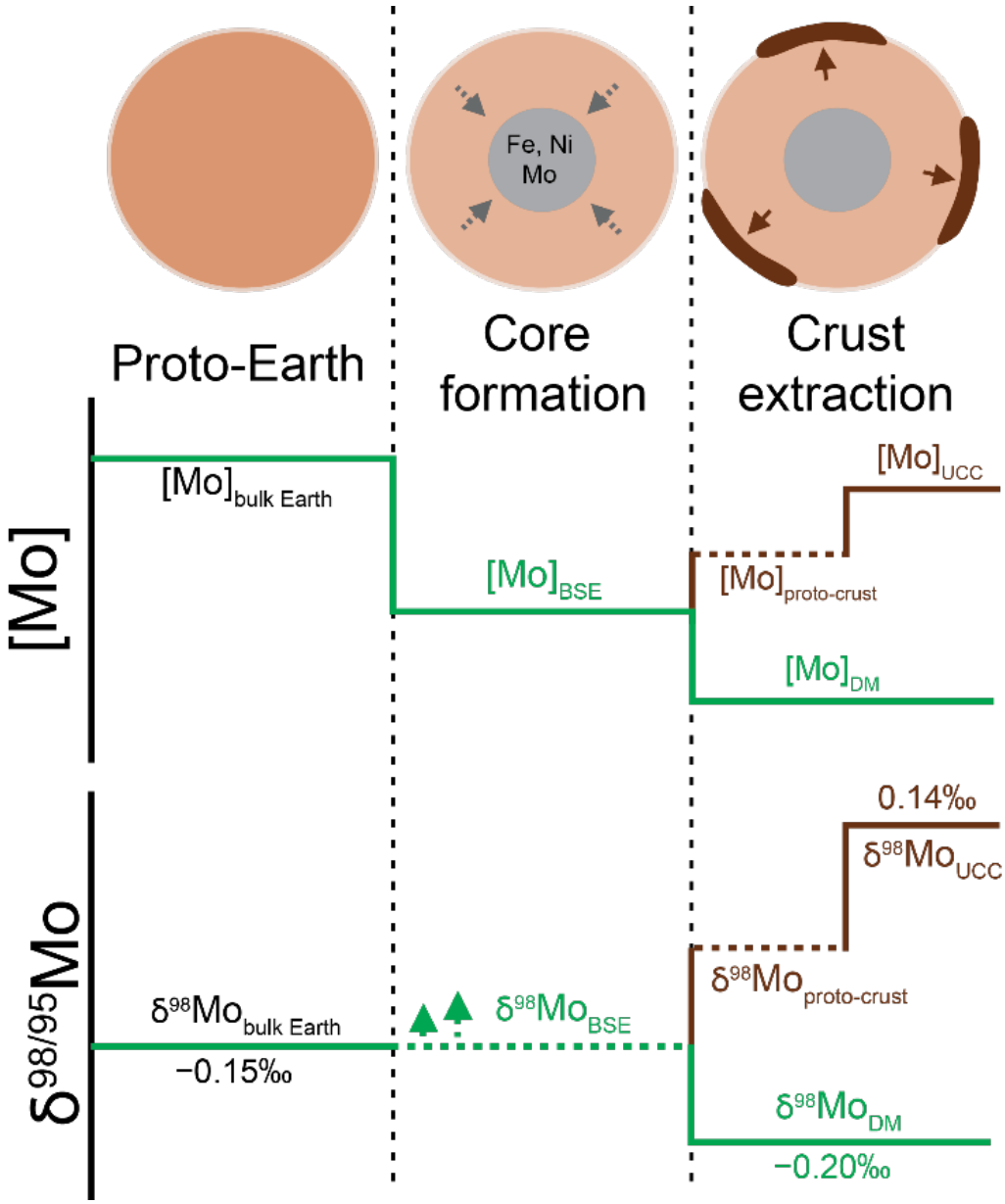

404

405 **Figure 2:** Schematic Mo evolution of Earth's mantle and crust during planetary

406 differentiation. Earth accretes from chondritic meteorites thus the bulk Earth initial δ^{98}Mo

407 will be chondritic. During core formation 95 % of Earth's Mo is sequestered into the core

408 trapping isotopically light Mo in the metal phase, possibly making the residual BSE heavier.

409 Subsequent extraction of Earth's isotopically heavy crust prior to 3.5 Ga resulted in a bulk

410 mantle that is lighter than the building blocks of Earth. Earth's earliest crust was more mafic

411 than modern crust and therefore had a different Mo concentration and isotopic composition.

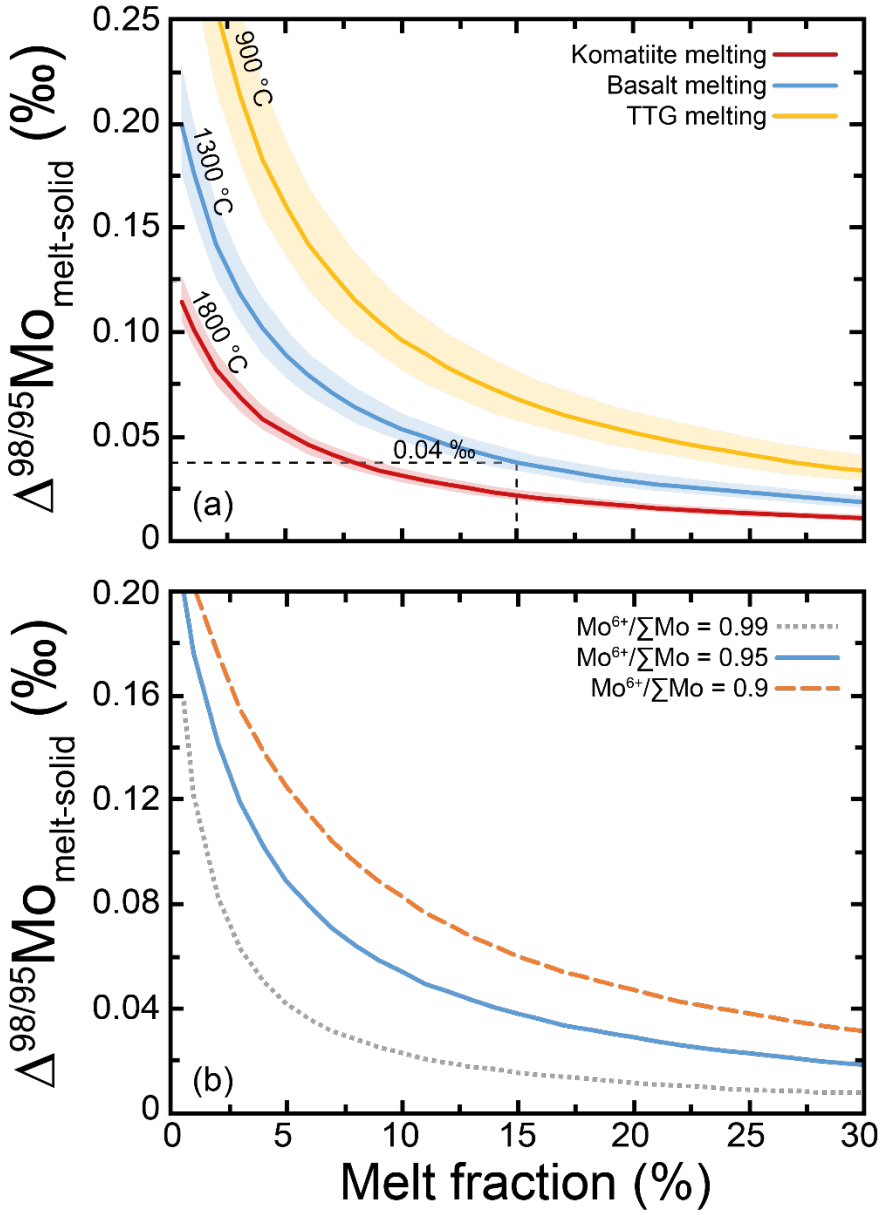

412

413 **Figure 3:** Partial melting model showing that the degree of enrichment of heavy Mo isotopes
414 in the melt phase is controlled by both temperature and the valance state of Mo. (a) the effect
415 of varying temperature at a constant oxygen fugacity ($Mo^{6+}/\sum Mo = 0.95$). Shaded areas
416 represent varying the temperature by ±100 °C. (b) The effect of varying oxygen fugacity at a
417 constant temperature (1300 °C).

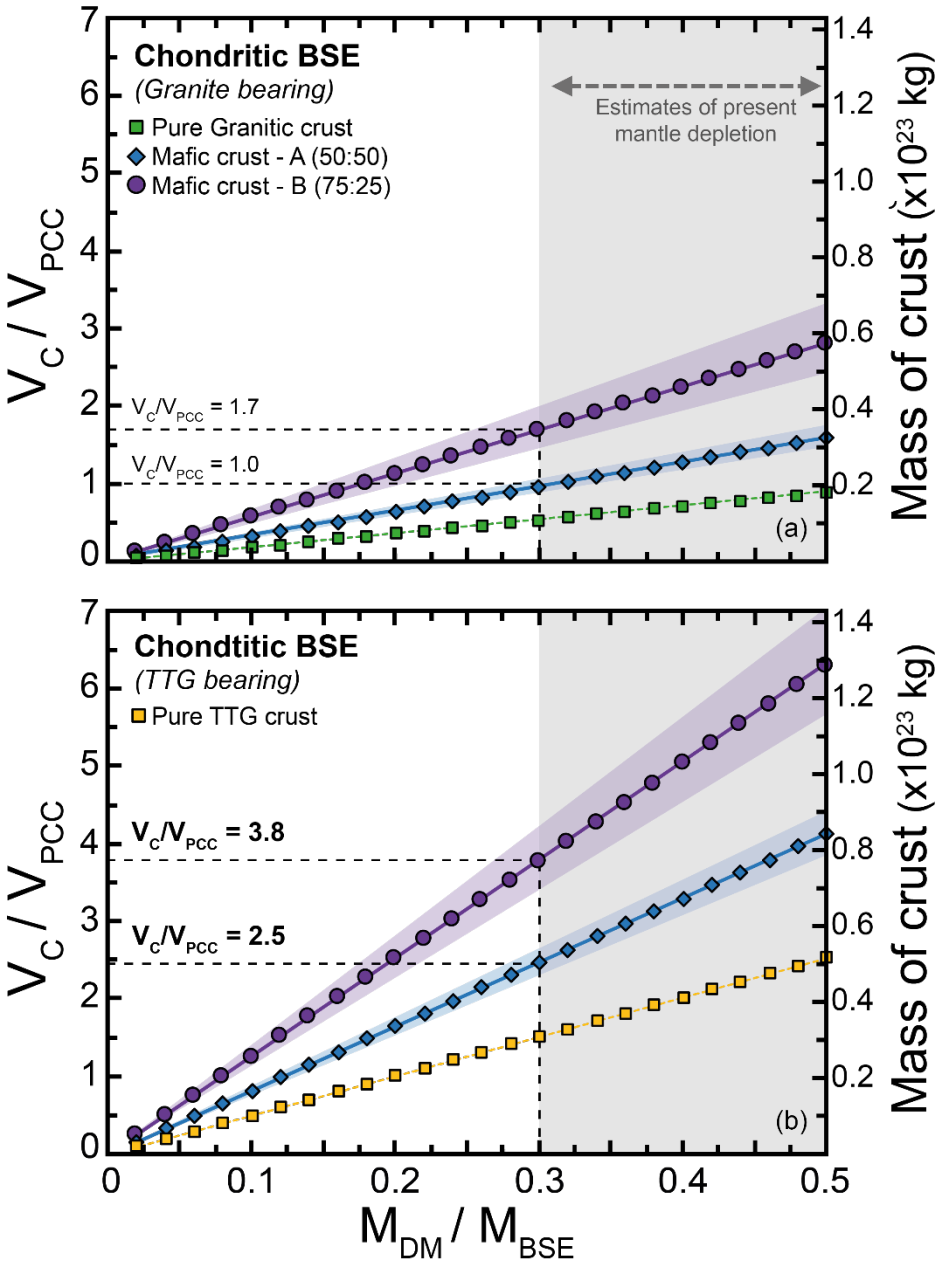

418

419 **Figure 4:** Results of Mo isotope mass balance calculations which estimate the mass of crust
420 extraction required to balance the composition of the depleted mantle. This mass of crust can
421 then be converted into a volume of crust (V_C) relative to the present volume of continental
422 crust (V_{PCC}) and varies depending on the proportion of the total BSE that has undergone melt
423 depletion (M_{DM}/M_{BSE}). Mafic crust-A and -B contain mafic and felsic rocks in 50:50 and
424 75:25 ratios, respectively. The shaded areas represent varying the proportions of the two
425 endmembers by ±5%.

426

Supplementary information for:

Molybdenum isotope evidence for extensive crustal extraction and recycling in Earth's first billion years

Alex J. McCoy-West[1, 2], Priyadarshi Chowdhury[2], Kevin W. Burton[1], Paolo Sossi[3], Geoff M. Nowell[1], J. Godfrey Fitton[4], Andrew Kerr[5], Peter A. Cawood[2] and Helen M. Williams[1,6]

[1]Department of Earth Sciences, Durham University, Elvet Hill, Durham DH1 3LE, UK
[2]School of Earth, Atmosphere and Environment, Monash University, Clayton, Victoria, 3800, Australia
[3]Institute of Geochemistry and Petrology, ETH Zürich
[4]School of GeoSciences, University of Edinburgh, Edinburgh EH9 3FE, UK
[5]School of Earth and Ocean Sciences, Cardiff University, Park Place, Cardiff CF10 3AT, UK
[6]Department of Earth Sciences, University of Cambridge, Downing Street, Cambridge CB2 3EQ, UK

Corresponding author: Alex McCoy-West (alex.mccoywest@monash.edu)

Figures and Tables

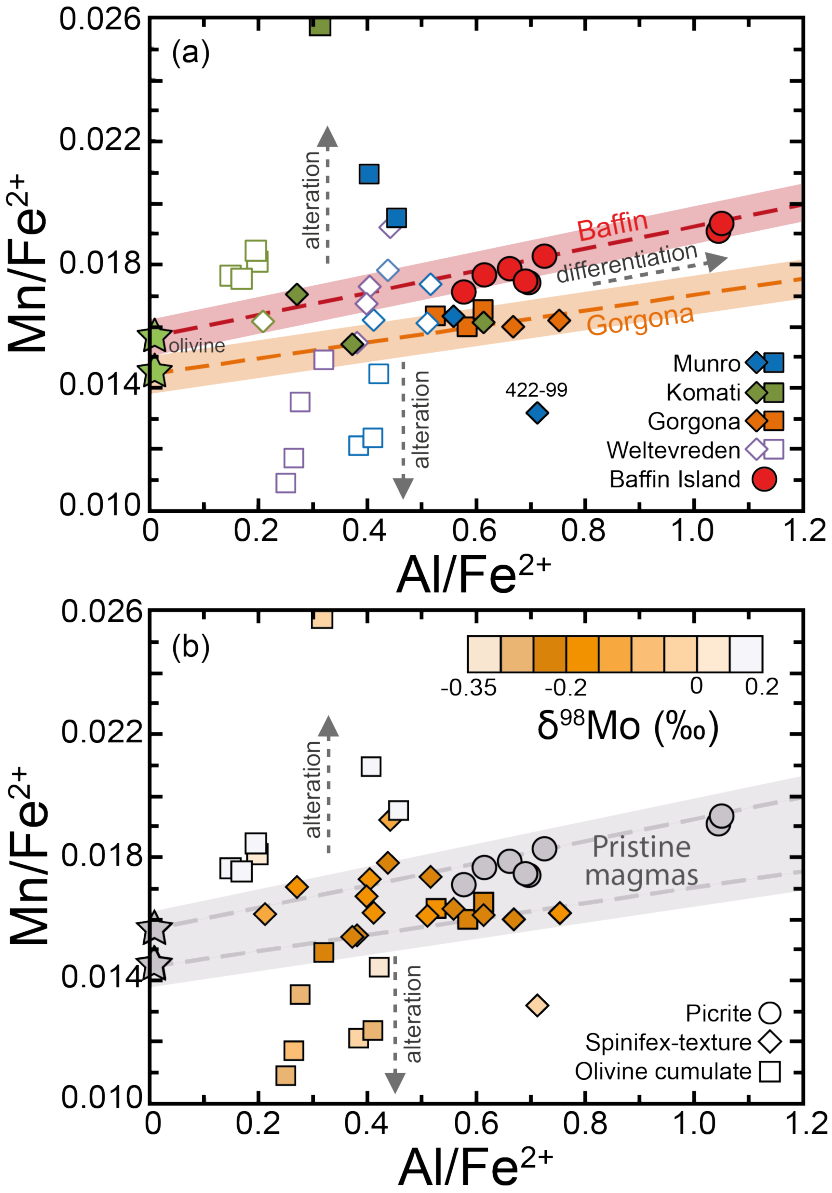

Supplementary Figure 1: Variation of Mn/Fe^{2+} versus Al/Fe^{2+} in komatiites and picrites. This type of plot is commonly used to assess alteration in komatiites [1,2]. Different rock types are distinguished: picrites (circles), spinifex textured (diamonds) and olivine cumulates (squares). (A) Filled symbols represent samples analysed herein with hollow symbols samples measured in Greber, et al. [3,4]. Major element data comes from refs. [5-11]. The shaded red and orange fields represent pristine unaltered samples, based on Baffin Island picrites and Gorgona komatiites, with variations the result of accumulation or fractional crystallization of olivine crystals. Samples that fall perpendicular to this trend have experienced elemental mobility and are considered altered. (B) Archean komatiite data is coloured based on the $\delta^{98}Mo$ of the samples. Gradational scale uses 0.05‰ increments from and −0.35 to 0‰, and 0.1‰ increments above 0‰. All samples with $\delta^{98}Mo \geq 0.1$‰ are plotted with the light grey on the righthand side. Notably, samples with $\delta^{98}Mo$ between −0.25 and −0.15‰ plot near the unaltered field defined by the Baffin Island and Gorgona magmas.

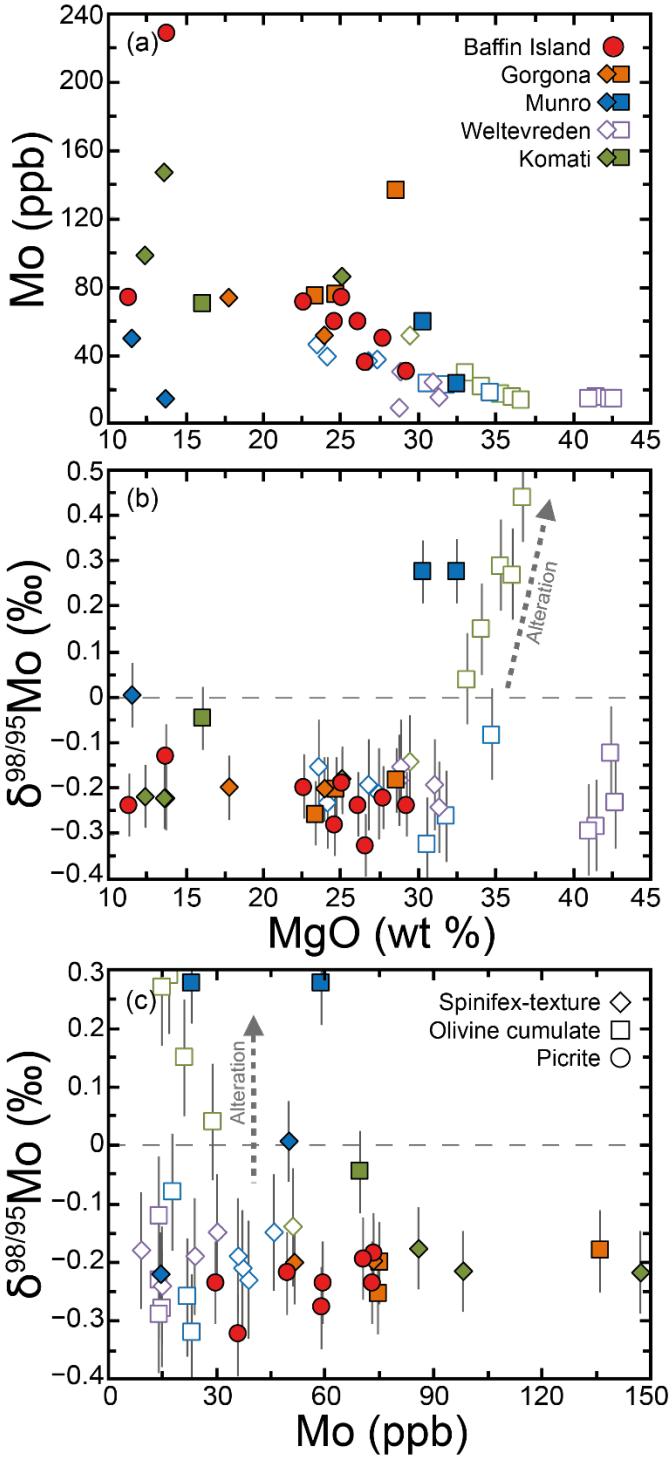

Supplementary Figure 2: Variation diagrams showing the MgO content, Mo concentration and δ^{98}Mo of komatiites and picrites. Filled symbols represent data analysed herein with hollow symbols samples investigated in Greber, et al. [3]. Error bars on δ^{98}Mo are the average reproducibility of the Baffin Island analyses (± 0.07‰). No resolvable covariation is obseved between δ^{98}Mo and MgO content. Notably, most spinfex texture lavas produce indentical δ^{98}Mo within anlytical errors at a wide range of Mo concentration, whereas the olivine cumulates have invariable Mo concentrations but more variation in δ^{98}Mo due to their greater proportion of olivine which is suspectibility to alteration.

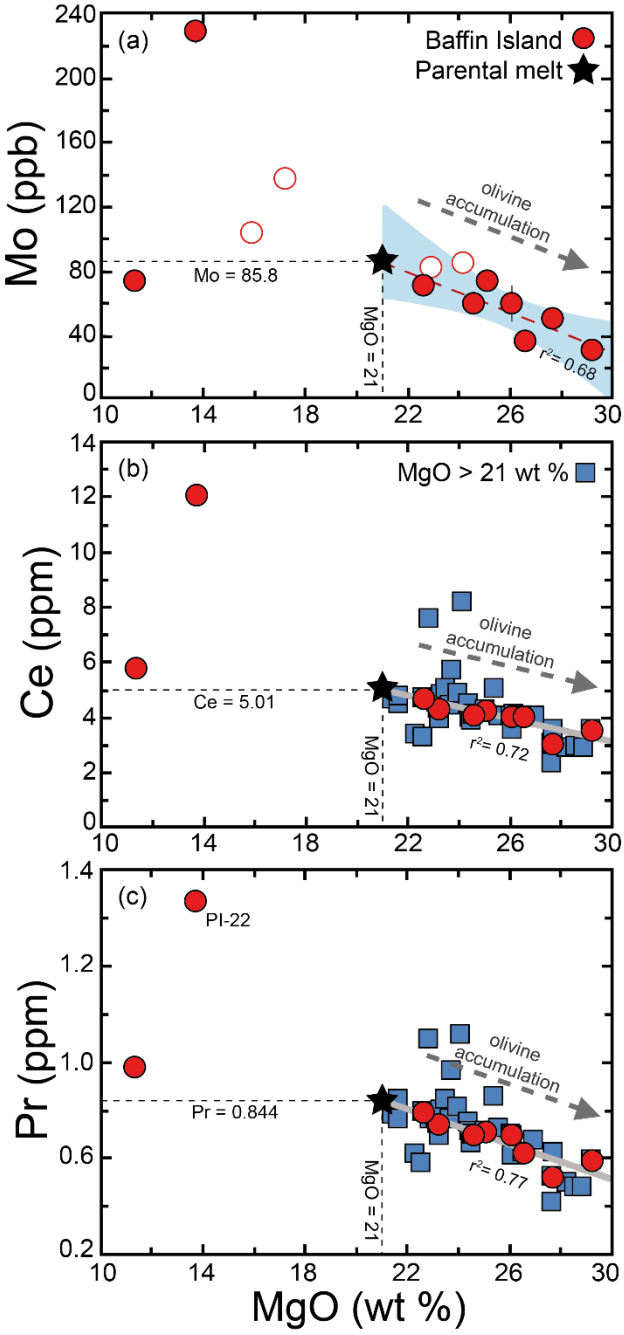

Supplementary Figure 3: Trace element evidence for olivine accumulation in high-MgO Baffin Island picrites. Excellent correlations are observed against MgO in samples with >21 wt % MgO. (a) Variation of Mo concentration versus MgO content. Hollow symbols are samples with only concentration data. Shaded area represents the 95% confidence interval of the correlation. (b-c) Ce and Pr concentration, respectively, versus MgO content. Whole rock data comes from Starkey, et al. [7] with the complete Baffin Island dataset (squares) plotted for comparison. The parental melt (i.e. the original composition of the magmas from the mantle source region corrected for olivine accumulation) at Baffin Island was calculated to have 21 wt % MgO (see McCoy-West, et al. [12] for detailed discussion).

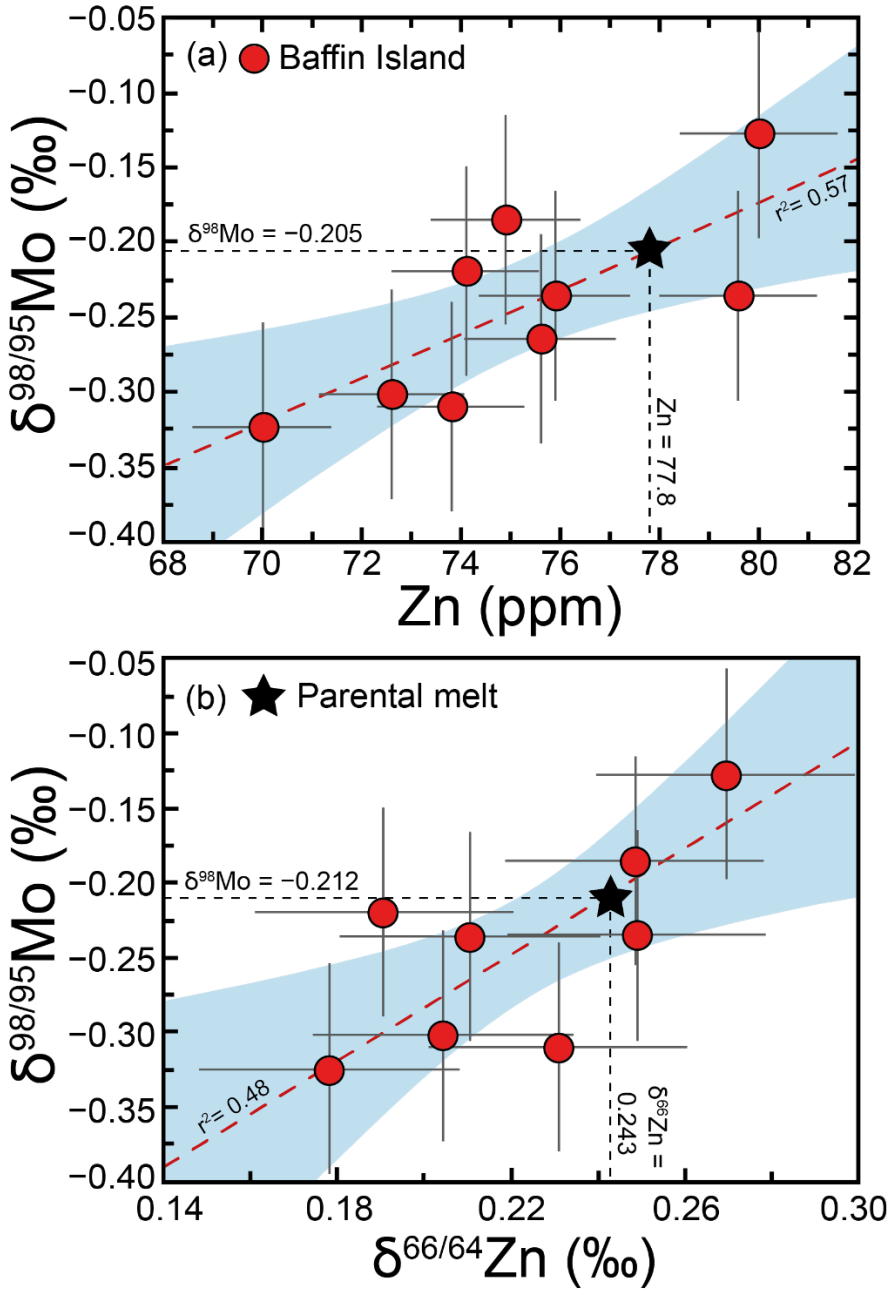

Supplementary Figure 4: Variation diagrams of δ^{98}Mo versus Zn concentration (a) and δ^{66}Zn (b). Comparative Zn data come from Starkey, et al. [7] and McCoy-West, et al. [12]. Shaded area represents the 95% confidence interval of the correlation. Error bars on δ^{98}Mo are the average reproducibility of the Baffin Island analyses (± 0.07‰), with errors on Zn concentration assumed to be 2% and δ^{66}Zn the long-term reproducibility (± 0.03‰). The correlation between Zn concentration and δ^{66}Zn and the Mo isotope compositions suggests that the variability is controlled by the same process (i.e. olivine accumulation). See McCoy-West, et al. [12] for more detailed discussion of the accumulation of olvine phenocrsyts that have experienced kinetic isotope exchange based on Fe and Zn isotopes.

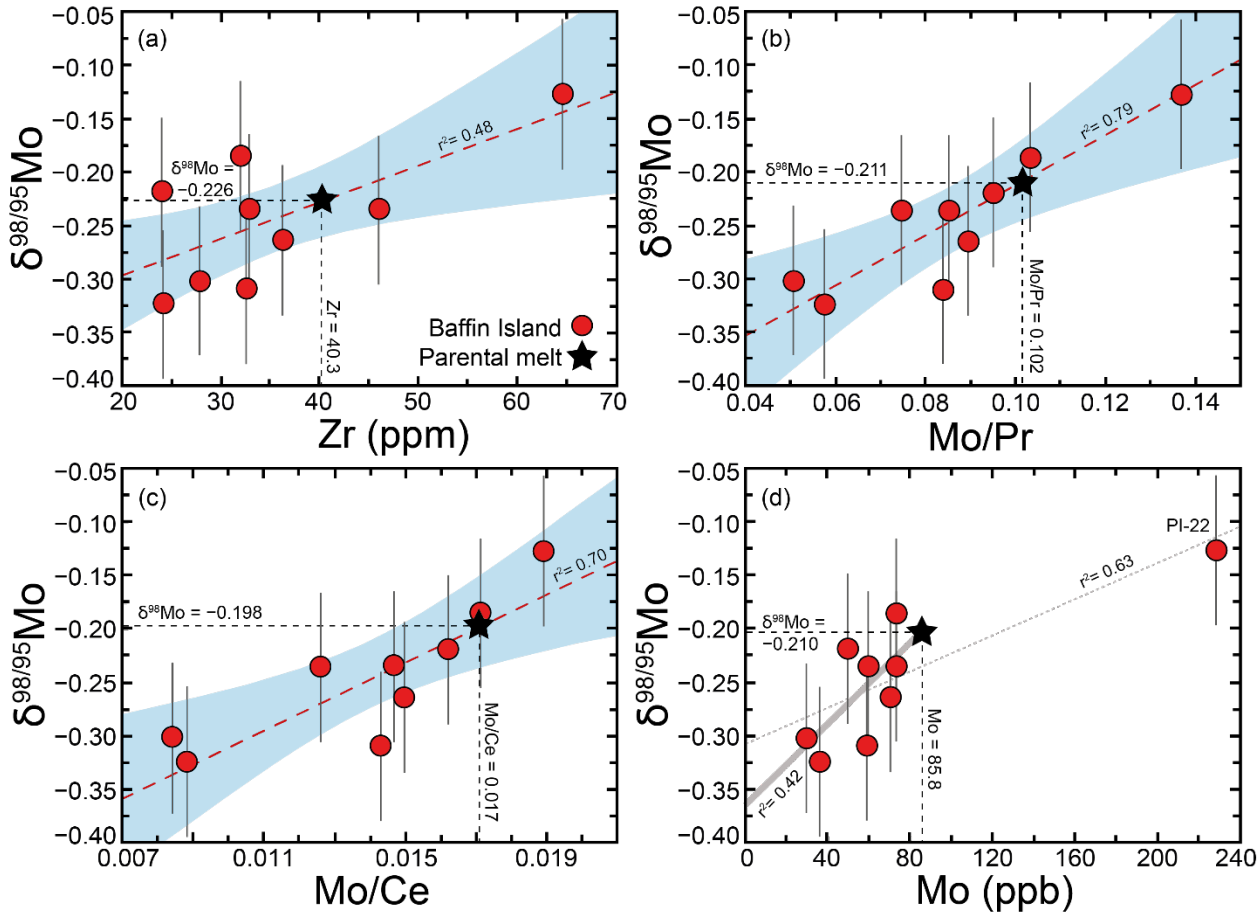

Supplementary Figure 5: Variation diagrams of δ^{98}Mo versus trace element concentrations or elemental ratios in the Baffin Island picrites. Comparative data come from Starkey, et al. [7]. Shaded areas represent the 95% confidence interval on the correlations. Error bars on δ^{98}Mo are the average reproducibility of the analyses (± 0.07‰). The strong correlations between MgO content and trace elements (see Fig. S4) allow calculation of the elemental concentration of the parental melt (i.e. 21 wt % MgO). This value is then used with the correlations presented above to obtain the δ^{98}Mo of the parental melt (see Table S2). The strong linear trends show this is the result of accumulation (i.e. a linear addition process) rather than magmatic differentiation (where parabolic curves would be expected).

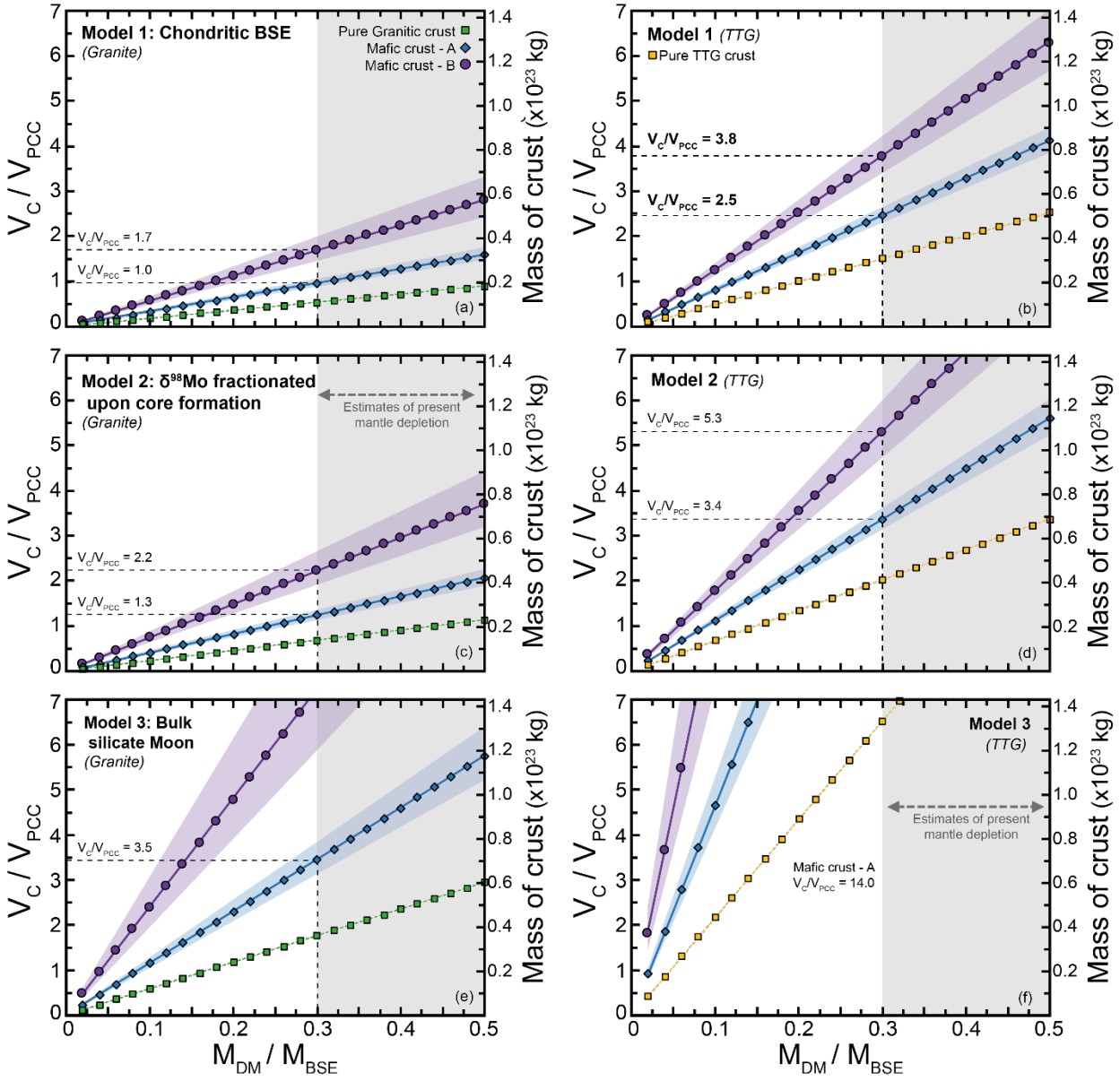

Supplementary Figure 6: Results of Mo isotope mass balance calculations which estimate the mass of crust extraction required to balance the composition of the depleted mantle. This mass of crust can then be converted into a volume of crust (V_C) relative to the present volume of continental crust (V_{PCC}) and varies depending on the proportion of the total BSE that has undergone melt depletion (M_{DM}/M_{BSE}). Thirty-fifty % depletion of the mantle (grey field) can reproduce the radiogenic isotope and incompatible element signatures of the crust and depleted mantle, assuming they represent complementary reservoirs [10,11,13,14]. (a-b) Model 1: assumes a chondritic BSE for Mo isotopes (δ^{98}Mo = −0.154‰); (c-d) Model 2: assumes an isotopically heavier BSE following core formation (δ^{98}Mo = −0.142‰). (c) Model 3: assumes the BSE equilibrate with the composition of the silicate Moon (δ^{98}Mo = −0.078 ‰). Crustal volumes are calculated for three different Archean crust types: a purely felsic crust, Mafic crust-A (minimum based on a mafic crust) and Mafic crust-B (a likely Archean crustal composition). Felsic-crust is composed exclusively of felsic rocks, while the Mafic crust-A and -B contain mafic and felsic rocks in 50:50 and 75:25 ratios, respectively. The felsic endmember is either granite (left side: a, c, e) or more realistic for the early Earth has a TTG composition (b, d, f; see Table S5 for further details).

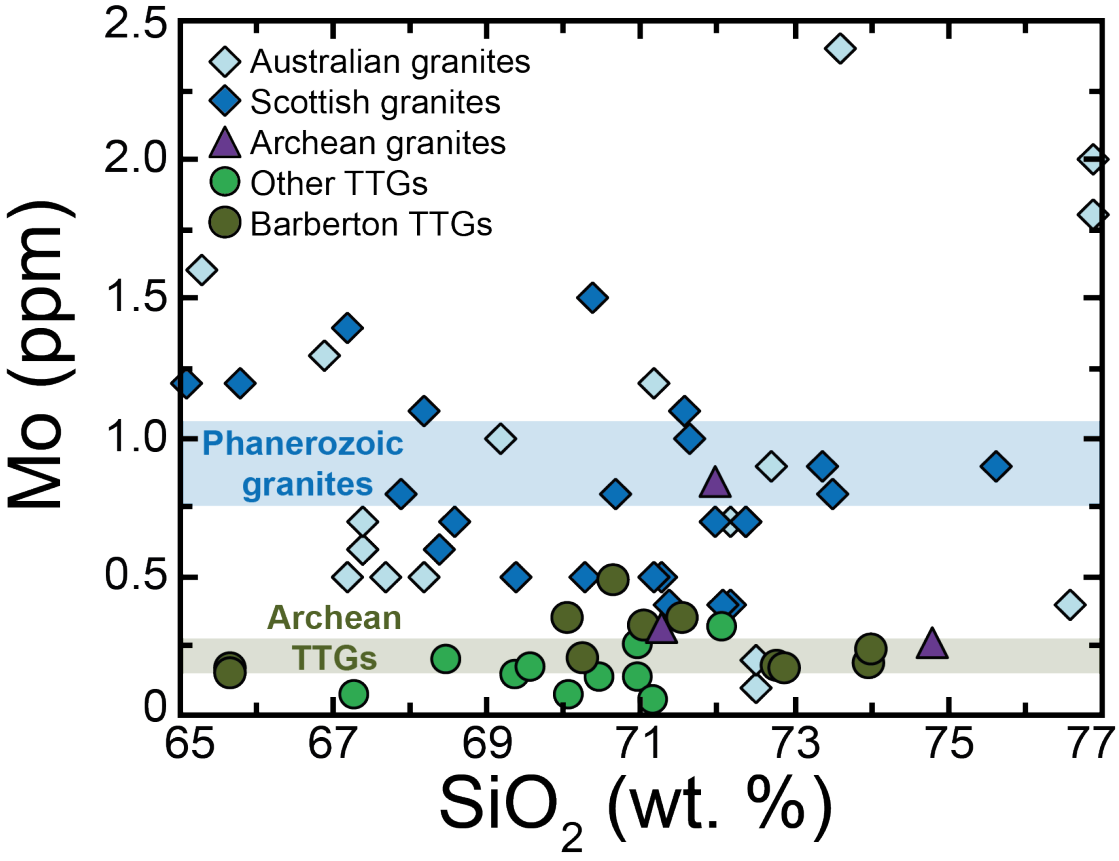

Supplementary Figure 7: Comparison of the Mo concentration of Phanerozoic granites and Archean granites and tonalite-trondhjemite-granodiorites (TTGs). Archean samples come from Greaney, et al. [15] and are divided into Barberton TTGs (3.2-3.6 Ga), other TTGs (Zimbabwe and Superior; 2.7-3.0 Ga) and granites (2.6-2.7 Ga). Phanerozoic samples come from Yang, et al. [16], they are divided on the basis of location into Australian (Lachlan and New England orogens; 286-428 Ma) and Scottish (Caledonian plutons; 392-408 Ma) samples. Shaded bars represent the averages for Archean TTGs (Mo = 0.21 ± 0.05 ppm; n = 26; [15]) and Phanerozoic granites (Mo = 0.90 ± 0.15 ppm; n = 46; [16]).

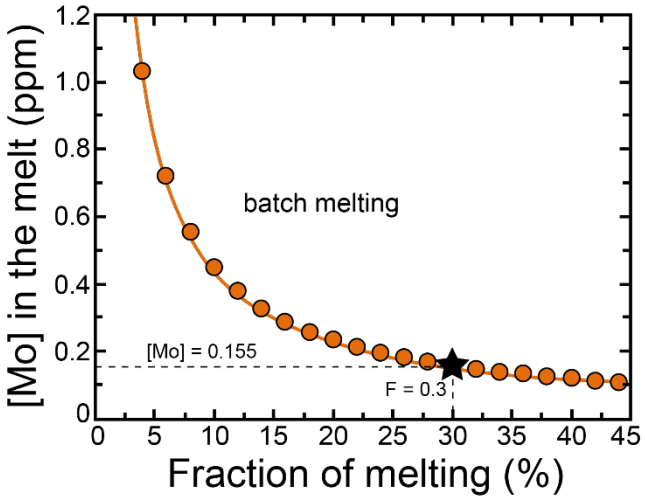

Supplementary Figure 8: Batch melting model show the variation in Mo concentration as a function of melt fraction. Modelling uses a bulk D_{Mo} of 0.006 [17] and assumes a source concentration of 0.047 ppm [18].
The [Mo] of the basalt endmember (0.155) is based on 30% melting of the mantle (sitting in the middle of the Archean range to produce a high Mg basalt; [19,20])

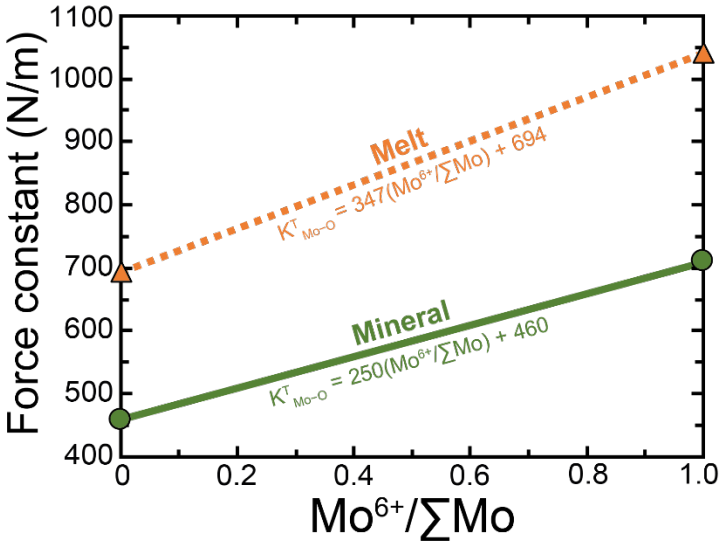

Supplementary Figure 9: Force constant of Mo−O bonds in minerals and melt as a function of $Mo^{6+}/\sum Mo$ used in the modelling presented in Figure 4. Based on values presented in Table S7.

Supplementary Table 1: Molybdenum concentrations and isotope compositions of high-degree partial melts and reference materials.

Sample	Location	Rock Type	MgO (wt%)	Mo (ng/g)			$\delta^{98/95}$Mo			*n*
				a	b	Average	a	b	Average	
Baffin Island										
PI-22	*Padloping*	pic	13.7	226.0	231.4	229 ±7.6	−0.092	−0.162	−0.127 ±0.098	*2*
PI-24	*Island*	pic	26.1	55.6	63.5	59.6 ±11.2	−0.243	−0.227	−0.235 ±0.023	*2*
PI-25		pic	27.7	49.6	49.3	49.4 ±0.4	−0.181	−0.257*	−0.219 ±0.107	*2*
PI-26		pic	25.1	74.0	72.7	73.3 ±1.8	−0.169	−0.202*	−0.186 ±0.047	*2*
PI-28		pic	11.3	75.4	73.0	73.0 ±3.4	−0.244	−0.227*	−0.236 ±0.024	*2*
PI-31~		pic	22.6	69.8	71.3	70.5 ±2.2	−0.333	−0.195	−0.264 ±0.195	*2*
PI-37		pic	26.6	35.9	35.6	35.8 ±0.4	−0.305	−0.343*	−0.324 ±0.054	*2*
PI-40~		pic	29.2	30.0	29.6	29.8 ±0.6	−0.235	−0.369*	−0.302 ±0.189	*2*
PI-43		pic	24.6	58.5	59.0	58.8 ±0.6	−0.342	−0.278*	−0.310 ±0.090	*2*
PAD-6^		pic	17.6	137.1	-					
DI-23^	*Durban*	pic	24.1	84.8	-					
DI-26^	*Island*	pic	15.9	102.9	-					
DUR-8^		pic	22.9	82.1	-					
Gorgona										
GOR94-29	*Gorgona*	STK	17.8	73.3			−0.197	-	−0.197 ±0.070	
GOR94-43	*Island*	STK	23.9	49.6	53.1	51.4 ±4.9	−0.213	−0.189	−0.201 ±0.034	*2*
GOR94-3		OC	28.6	135.8			−0.181	-	−0.181 ±0.070	
GOR94-17		OC	23.4	74.6			−0.254	-	−0.254 ±0.070	
GOR94-44		OC	24.7	75.2			−0.201	-	−0.201 ±0.070	
Lower Komati										
331/777a	*Komati*	STK	25.1	85.7	87.8	86.7 ±3.0	−0.169	−0.184	−0.177 ±0.021	*2*
331/778		STB	12.3	98.3	-		−0.216	-	−0.216 ±0.070	
331/786		STB	13.6	147.1	-		−0.218	-	−0.218 ±0.070	
331/790#	*Mundt's Concession*	OC	16.1	69.6	60.3	64.9 ± 13.1	−0.070	−0.020	−0.045 ±0.070	*2*
Munro										
422/84#	*Pyke Hill*	OC	30.3	59.1	-		0.276	-	0.276 ±0.070	
422/86#		OC	32.4	23.1	-		0.277	-	0.277 ±0.070	
422/99#		STB	11.5	49.9	-		0.007	-	0.007 ±0.070	
RL-12-1	*Red Lake*	STB	13.7	14.4	22.2	18.2 ±10.7	−0.242	−0.198	−0.220 ±0.062	*2*
Mid-ocean ridge basalt										
45N	*Mid-Atlantic*	E-type		403	418	410 ±21	−0.198	−0.119	−0.159 ±0.056	*2*
Rock Standards										
AGV-1	*Oregon*	and	1.5	2186	2062	2101	−0.154	−0.168		
				2055		±147	−0.169		−0.164 ±0.017	*3*
BCR-1	*Oregon*	bas	3.5	1741	1676	1682	0.066	0.076		
				1630		±111	0.079		0.074 ±0.013	*3*
BIR-1	*Iceland*	bas	9.7	32.2	34.1	33.1 ±2.6	−0.111	−0.155	−0.133 ±0.062	*2*
BHVO-1	*Hawaii*	bas	7.2	1077	1092		−0.219	−0.220		
				1025	1103	1061	−0.205	−0.182		
				1006		±85	−0.200		−0.205 ±0.031	*5*

Errors on average Mo concentrations and $\delta^{98/95}$Mo are two-standard deviations. For samples with only one replicate the average reproducibility of the Baffin Island samples is taken as the error (± 0.07 ‰; see the methods section for further discussion). Sample types: pic = picrite; OC = olivine cumulate; STK = spinifex texture komatiite; STB = spinifex texture basalt; bas = basalt; and =andesite. # samples are altered and not included in calculating the average composition of Archean komatiites. * denotes samples that were digested initially using carius tube digestion then followed by HF-HNO_3 digestion. ^ samples that were only run initially for concentrations by isotope dilution. ~ Two samples did not reproduce very well and the 2 s.d. are large, however, the total range between the replicates is significantly smaller.

Supplementary Table 2: Calculation of the Mo isotope composition of the Baffin Island parental melt

Parameter	Regressions	Value at 21 wt % MgO	$\delta^{98/95}$Mo (‰)
Zn (ppm)	Fig. S2 (r^2 = 0.57)	77.8	−0.205 ±0.040
δ^{66}Zn (‰)	Fig. S2 (r^2 = 0.48)	0.243	−0.212 ±0.050
Mo/Pr	Fig. 2 (r^2 = 0.79)	0.102	−0.211 ±0.043
Mo/Ce	Fig. S4 (r^2 = 0.70)	0.017	−0.198 ±0.043
Zr (ppm)	Fig. S4 (r^2 = 0.48)	40.3	−0.226 ±0.035
Mo (ppb)	Fig. S4 (r^2 = 0.42)	85.8	−0.210 ±0.068
		Average Parental Melt:	**−0.210 ± 0.010**

Errors on δ^{98}Mo are calculated from the 95 % confidence interval (error envelopes) on the regressions calculated using Isoplot [21] at the composition of the parental melt. The MgO content of the Baffin Island parental melt was calculated at 21 wt. % MgO using the inflection method (see McCoy-West, et al. [12]). Given the strong correlations between elemental concentration and MgO content in the picrites with >21 wt. % MgO, using linear regression concentrations of the elements of interest are calculated at the parental melt composition. Zn isotope data comes from McCoy-West, et al. [12]. Trace earth element data is from Starkey, et al. [7].

Supplementary Table 3: Locations and Mo isotope compositions of primitive materials used to calculate the Mo isotope composition of the accessible mantle

Location	$\delta^{98/95}$Mo (‰)	2 s.d.	*n*	References
Depleted-MORB				
Pacific-Antarctic Ridge	−0.206 ±0.021	±0.033	*5*	Bezard, et al. [22]
Phanerozoic picrite				
Baffin Island, NE Canada	−0.210 ±0.10	±0.019	*6*	Herein
Phanerozoic komatiite				
Gorgona, Columbia	−0.207 ±0.034	±0.055	*5*	Herein
Archean komatiites				
Komati, South Africa	−0.187 ±0.059	±0.074	*4*	Herein; Greber, et al. [3]
Weltevreden, South Africa	−0.215 ±0.038	±0.031	*4*	Greber, et al. [3]
Munro, Canada	−0.196 ±0.044	±0.070	*5*	Greber, et al. [3]; Herein
Mantle Xenoliths				
Tariat, Mongolia	−0.210 ±0.093	±0.177	*6*	Liang, et al. [23]
Vitim, Siberia	−0.198 ±0.061	±0.077	*4*	Liang, et al. [23]
Accessible Mantle	**−0.204 ±0.008**	**±0.018**	*8*	Herein

Errors on δ^{98}Mo are 95% standard errors (95% s.e. = t * s.d./(n)1/2, where t = inverse survival function of the Student's t-test at the 95% significance level and (n-1) degrees of freedom), with two-standard deviation (2 s.d.) also shown to represent population uncertainty. Depleted mid ocean ridge basalts (MORB) are only those samples with measured $^{143}Nd/^{144}Nd \geq 0.513117$. Mantle xenoliths from Kilbourne Hole, New Mexico were excluded due to their large spread in δ^{98}Mo values (0.32 ‰) and limited sample set (n = 3).

Supplementary Table 4: Molybdenum isotope compositions of geochemical reservoirs presented in Figure 1 or used in modelling

Reservoir	$\delta^{98/95}$Mo (‰)	2 s.d.	*n*	References

Chondrites	−0.154 ±0.013	±0.051	*18*	Liang, et al. [23], Burkhardt, et al. [24]
Archean komatiites	−0.199 ±0.019	±0.062	*13*	Herein
Mantle peridotites	−0.206 ±0.050	±0.180	*15*	Liang, et al. [23]
Global basalts	−0.10 ±0.04	±0.27	*57*	Yang, et al. [16] and therein
Global granites	0.16 ±0.05	±0.41	*55*	Yang, et al. [16] and therein
Upper Continental Crust	0.14 ±0.07		*112*	Yang, et al. [16]

Errors on δ^{98}Mo are 95% standard errors (95% s.e. = t * s.d./(n)1/2, where t = inverse survival function of the Student's t-test at the 95% significance level and (n-1) degrees of freedom), with two-standard deviation (2 s.d.) also shown to represent population uncertainty. Chondrite average excludes CK and CM groups meteorites. Upper continental crust composition was calculated assuming a 10:1 proportion of felsic to basaltic rocks [16].

Supplementary Table 5: Molybdenum concentration and isotopes compositions of geochemical reservoirs used in mass balance calculations

Reservoir	Mass (kg)[a]	Density (kg/m^3)	Mo (ppm)	$\delta^{98/95}$Mo (‰)
Chondrites			ca. 1.7[b]	−0.154 ±0.013[f,g]
Earth	5.9376 x 10^{24}			
Core	1.932 x 10^{24}		ca. 5[b]	−0.16 ±0.02[f]
Bulk silicate Earth	4.0603 x 10^{24}		0.047 ± 0.019[c]	−0.154
Mantle	4.0343 x 10^{24}			
Depleted mantle	Varied		0.025 ± 0.007[d]	−0.204 ±0.008
Modern crust	2.6 x 10^{22}			
Mafic endmember		3000	0.155	−0.10 ±0.04[h]
Types of Crust				
Granite bearing models				
Pure Granitic crust		2750	0.47[d]	0.16 ±0.07[h]
Mafic crust A (50:50)		2850 ± 15	0.313 ± 0.016	0.096 ± 0.010
Mafic crust B (75:25)		2925 ± 15	0.234 ± 0.016	0.031 ± 0.018
TTG bearing models				
Pure TTG crust		2750	0.28[d]	0.03
Mafic crust A (50:50)		2850 ± 15	0.218 ± 0.006	−0.016 ± 0.006
Mafic crust B (75:25)		2925 ± 15	0.186 ± 0.006	−0.051 ±0.008

Mafic crust compositions were calculated by mixing different proportions of mafic and felsic material (i.e. 75:25 is 75% mafic). Molybdenum concentration data shows that Phanerozoic granites are clearly more evolved than there Archean counterparts (see Fig. S7). The Mo concentration of the felsic endmembers were taken from the available published data in Greaney, et al. [15], using the average composition of the oldest 3.5 Ga Barberton TTGs (0.28; n = 15), and 2.7 Ga granites (0.47; n = 3) available. The Mo concentration of the mafic endmember (Mo = 0.155) was calculated based on batch melting of the bulk silicate Earth assuming an F of 0.3 (higher than today due to the elevated mantle temperatures in the Eoarchean) and a bulk D_{Mo} of 0.006 [17] (see Fig. S8). The isotopic composition of mafic endmember uses the modern global basalt average of δ^{98}Mo = −0.10 ±0.04 ‰ (n = 57). Partial melting is a time invariant process at constant temperature and therefore the modern basalts provide a good analogue. The partial melting model presented in Figure 4 shows that a melt will 0.05‰ heavier than the its mantle source (chondrite BSE) as required in this instance from 12-15 % melting. The formation of TTGs requires the remelting of metabasalt, given that TTGs have lower Mo concentrations than granites it is sensible to assume their δ^{98}Mo will also be less evolved. Here we have taken the simplest approach (i.e. two step formation of TTGs) and taken the average of global basalts and granites to estimate the δ^{98}Mo of TTG felsic component. Densities were calculated by mixing basaltic (3000 kg/m^3) and granitic (2700 kg/m^3) endmembers. Errors on Mafic crusts (A and B) represent varying the proportions of the two endmembers by 5%. References for other parameters as follows: a) Yoder [25]; b) McDonough [26]; c) Palme and O'Neill [18]; d) Salters and Stracke [27]; e) Rudnick and Gao [28]; f) Burkhardt, et al. [24]; g) Liang, et al. [23]; h) Yang, et al. [16].

Supplementary Table 6: Model parameters for the calculation of Mo isotope fractionation during non-modal batch melting

Phase	Starting fraction*	Melting reaction*	D_{Mo4+}^	D_{Mo6+}^
Olivine	0.6	−0.15	0.5	0.006

Orthopyroxene	0.25	0.15	0.7	0.009
Clinopyroxene	0.1	1.0	0.3	0.001

*Melting parameters come from Walter [29]. ^ Partition coefficients are taken from Leitzke, et al. [30]. Model assumes that the force constant is a linear function of $Mo^{6+}/\sum Mo$ for both minerals and melt and that all minerals have the same $Mo^{6+}/\sum Mo$. Modelling uses force constants calculated in Table S7.

Supplementary Table 7: Parameters used for the calculation of force constants of Mo isotopes in minerals and melts at varied oxidation state.

	$\overline{Z}_{Mo}$	$C_{N\,Mo}$	$\overline{S}_{Mo}$	$\overline{S}_{O}$	r_{Mo-O} (m)	$K_{f\,Mo-O}$ (N/m)	K^{T}_{Mo-O} (N/m)
Melt							
$Mo^{6+}O_4$ (2-)	6	4	1.5	0.5	1.76^{-10}	349.8	1040.8
$Mo^{4+}O_4$ (4-)	4	4	1.0	0.5	1.76^{-10}	233.2	693.9
Minerals							
$Mo^{6+}O_3$	6	6	1.0	0.5	2.00^{-10}	158.9	709.3
$Mo^{4+}O_2$	4	6	0.67	0.5	2.02^{-10}	102.8	459.0

$\overline{Z}_{Mo}$ = cation charge; C_N = coordination number. $\overline{S}_{Mo}$ and $\overline{S}_{O}$ is the average bond valence of molybdenum and oxygen, respectively. r_{Mo-O} = Bond length in meters. $K_{f\,Mo-O}$ = is the force constant approximated by solving the Born-Lande equation. K^{T}_{Mo-O} = is the total force constant corrected by a scaling factor related to the proportion of ionic bonds (the ionicity of the Mo−O bond based on the Pauling scale is 0.336). All formulas required for calculating force constants can be found in Sossi and O'Neill [31]. Molybdenum is VI-fold (octahedral) co-ordinated in minerals [32,33] and predominantly IV-fold (tetrahedral) in silicate melts [34]. The main uncertainty comes from the bond length of Mo in mineral phases (e.g. olivine, pyroxene), here we use the values for pure Mo oxides taken from Farges, et al. [34]. Given that Mo is a trace element it should have a similar bond length to Mg and Fe in olivine (2.05^{-10} m), which is comparable to that of the pure metals. Farges, et al. [34] also present the Mo−O bond length of sodium silicates melts which provides the best estimate of this parameter in basaltic melts.

Supplementary Table 8: Leaching experiments on Baffin Island picrites.

Sample	Whole Rock		Residue (Silicates)		Leachate (Non-silicates)	
	Mo (ng/g)	$\delta^{98/95}$Mo	Mo (ng)	$\delta^{98/95}$Mo	Mo (ng)	$\delta^{98/95}$Mo
PI-37	35.8	−0.324 ±0.054	~11	−0.323 ±0.054	~7	−0.403 ±0.051
PI-43	58.8	−0.310 ±0.090	~16	−0.263 ±0.026	~10	−0.374 ±0.034

A second aliquot of the same sample powder was sealed in a carius tube with 9 mL of reverse Aqua Regia (4:5 HCl-HNO3) and heated to 220˚C for >72 hours. Following cooling the Aqua Regia supernatant was removed (henceforth the leachate; predominantly chromite and any sulfides present) and the remaining residual material (henceforth the residue; predominantly silicates) were spiked and processed separately through chemistry.

Methods

Molybdenum separation

All chemical separations were undertaken within the Arthur Holmes Isotope Geochemistry Laboratories at Durham University. The samples analysed herein have previously been extensively characterised Baffin Island [12,35] and Archaean Komatiites [8,36] with all powders created in Agate mills. Between 0.1-1.1 g of whole rock powder was weighed out to obtain ca. 30-150 ng of natural Mo and spiked with an equal amount of a ^{97}Mo–^{100}Mo double-spike to yield the ideal spike sample ratio of 1:1 [37]. Two digestion methods were implemented in this study: 1) Most samples were digested in 15 mL Savillex beakers containing a 3:1 mixture of 29M HF + 16M HNO_3 on a hotplate at 130ºC for ≥72 hours. Following evaporation, the samples were refluxed several times in 16M HNO_3 and 6M HCl to ensure complete decomposition of fluorides. For any samples that contained visible chromite or spinel grains the dissolved silicate portion was removed and saved, and an additional Parr bomb digestion step was undertaken to completely dissolve any refractory minerals. 2) Alternatively, carius tubes digestions were undertaken on some Baffin Island samples whereby ~1.0 g of sample powder was double spiked and mixed with 9 mL of reverse Aqua Regia (4:5 HCl-HNO_3), the tubes were subsequently sealed and heated to 220˚C for >72 hours. Following cooling the carius tubes were opened and the supernatant and all undissolved silicate material was removed, using multiple rinses with MQ H_2O. This material was then further processed with a conventional HF-HNO_3 hotplate digestion, to dissolve the refractory silicate portion.

A leaching experiment was undertaken on two of the Baffin Island picrites (PI-37, PI-43). A second aliquot of the same sample powder was sealed in a carius tube with 9 mL of reverse Aqua Regia (4:5 HCl-HNO_3) and heated to 220˚C for >72 hours. Following cooling

669 the Aqua Regia supernatant was removed (henceforth the leachate; predominantly chromite
670 and any sulfides present) and the remaining residual material (henceforth the residue;
671 predominantly silicates) was then rinsed three times with MQ H_2O. The residue was then
672 dried for reweighing and subsequently digested using conventional HF-HNO_3 digestion as
673 described above. When fully dissolved the concentration of Mo in the two splits was
674 obtained and the samples were spiked using the ^{97}Mo–^{100}Mo double spike and then refluxed
675 several times in concentrated HNO_3 to equilibrate the spike and sample.

676 Chemical separation of Mo was achieved using anion exchange (AG1-x8)
677 chromatography following the procedure described by Willbold, et al. [38]. The samples are
678 loaded onto the columns in 5 mL of 3M HCl + 0.05M ascorbic acid, the addition of ascorbic
679 acid coverts Fe^{3+} to Fe^{2+} which aids in elution of Fe from the anion exchange resin. This
680 reaction is accompanied by a colour change from yellow to colourless when the reaction has
681 been complete. Prior to loading all sample solutions were transferred into 15 mL centrifuge
682 vials and centrifuged to remove any precipitates that may have formed in the dilute HCl
683 loading solution. The sample matrix is then eluted in 3 mL of 3M HCl, 13 mL of 0.5M HCl
684 + 0.5% H_2O_2, 10 mL of 1M HF and 3 mL of MQ H_2O, prior to collection of the purified Mo
685 fraction in 12 mL of 1M HCl. Larger samples with >0.5g of material were loaded onto the
686 columns in 10-15 mL of 3M HCl to ensure complete dissolution of the samples. These high
687 mass samples were also processed through the complete chemical separation procedure twice
688 to ensure the complete removal of Fe and Ru that can provide isobaric interferences during
689 mass spectrometry. Total Mo procedural blanks calculated following double-spike
690 deconvolution range from 0.18 to 0.40 ng (n = 7) and are considered negligible.

691 *Mass Spectrometry*

692 Molybdenum isotope compositions were measured using a Thermo-Finnigan Neptune multi-
693 collector induction coupled plasma mass spectrometers (MC-ICP-MS). Samples were

694 introduced using an Aridus II desolvating nebuliser and a low uptake rate Cetac35 nebuliser
695 (aspiration rate 25-35 $\mu l min^{-1}$). All measurements were made in low resolution using X-
696 cones, and static collection mode with the simultaneous measurement of 9 isotopes ^{91}Zr,
697 ^{92}Mo, ^{94}Mo, ^{95}Mo, ^{96}Mo, ^{97}Mo, ^{98}Mo, ^{99}Ru and ^{100}Mo. Standard operation involved
698 introduction of 150 ppb Mo double-spiked solutions in 0.5M HNO_3 with trace HF and
699 produced a maximum sensitivity was ~380 $Vppm^{-1}$. Each analysis consisted of 1 block of
700 50 cycles with a 4 s integration time and was immediately preceded by the analysis of an acid
701 blank, with a washout of 180 s occurring after each sample. Due to the low aspiration rate a
702 single analysis used <200 µl of solution. All Mo isotope measurements herein are reported
703 relative to the internationally accepted reference solution the National Institute of Standards
704 and Technology (NIST) SRM3134 [39,40] where $\delta^{98}Mo = 0‰$ as convention dictates. In all
705 cases, conventional delta (δ) notation is used to express the ratios:

706 $$\delta^{98/95}Mo = [(({}^{98}Mo/{}^{95}Mo)_{SAMPLE}/({}^{98}Mo/{}^{95}Mo)_{NIST\ 3134}) - 1] \times 1000 \quad (1)$$

707 Data reduction was carried out using the Isospike plugin [41] for Iolite [42] which is underpinned
708 by the double spike deconvolution equations of Rudge, et al. [37]. Baseline subtraction was
709 undertaken using the 60 s of acid blank that immediately preceded a sample, with direct
710 isobaric interferences from Zr on ^{92}Mo, ^{94}Mo and ^{96}Mo and Ru on ^{96}Mo, ^{98}Mo and ^{100}Mo
711 mass fractionation corrected iteratively using the beta-factors calculated following the initial
712 deconvolution. In addition to using the double spike to correct for instrumental mass
713 fractionation, a secondary correction for within run mass spectrometer drift was applied using
714 IsoSpike. The Mo isotope compositions of the unknowns were corrected using linear
715 interpolation by adjusting the composition of the bracketing analyses of the primary standard
716 NIST3134, run at least every two unknowns, to 0‰.

717 The long-term stability of the mass spectrometer over a two-year period was
718 confirmed by repeated measurement of the in-house standard Romil which has an average

719 δ^{98}Mo of 0.045 ± 0.027‰ (2 s.d.; n = 327). Long-term accuracy was tested by repeated
720 analyses of international standard solutions Open University (–0.341 ± 0.032‰, n = 58) and
721 Bern (–0.242 ± 0.029‰, n = 73), which are within error of previous determinations [40,43]. The
722 reproducibility of analyses was further evaluated using a range of US Geological Survey rock
723 standards. A range of first generation rock standards (BCR-1, BHVO-1, and AGV-1) were
724 analysed here (see Table 1), multiple digestions (n = 3-5) reproduce to better than 0.031‰,
725 however, both BCR-1 and BHVO-1 have lower Mo concentrations and distinctly different
726 δ^{98}Mo than there second generation counterparts (i.e. BHVO-2) [24,44,45], which suggests that
727 these samples were contaminated with Mo during preparation of the second aliquot as
728 suggested previously [38,46]. Two separate digestions of low Mo (~30 ng/g) standard BIR-1
729 yield an average δ^{98}Mo of –0.133 ±0.062‰, which is within error of the previous estimate [38].
730 Replicate digestions of the high mass, low Mo (30-75 ng/g) Baffin Island and komatiite
731 samples herein generally reproduce to better than ±0.10‰, with two samples having
732 significantly larger 2 s.d. (the statistics are poor with only two replicates) although their total
733 range in δ^{98}Mo is <0.14‰. Therefore, we conservatively consider ± 0.07‰ as the long-term
734 reproducibility of the measurements herein (the average 2 s.d. variability on the replicates
735 herein is ± 0.068‰; n = 14).
736
737

738 **Mass balance calculations**

739 The distribution of δ^{98}Mo between the depleted mantle and crust after differentiation can be
740 estimated using isotopic and elemental mass balance (e.g. Willbold and Elliott [46]). The
741 equations presented here are similar to those used previously in Hofmann [47]. Here we
742 consider that Mo of a portion of the *bulk silicate Earth* (BSE) has been accessed for crust
743 formation and is distributed among two reservoirs; a *depleted mantle* (DM) and a *proto-crust*
744 (C) (see Fig. S10). Previous studies using radiogenic isotopes suggest that only 30-50 % of
745 whole mantle has been depleted [10,11,13,14], which suggests that the mass of mantle sampled is
746 less than that of whole BSE, i.e. $m_{DM} << m_{BSE}$, and $m_{DM} = m_{BSE}$ only if the whole BSE mass
747 has been used for crust extraction, which is probably not the case [10,11,13,14].

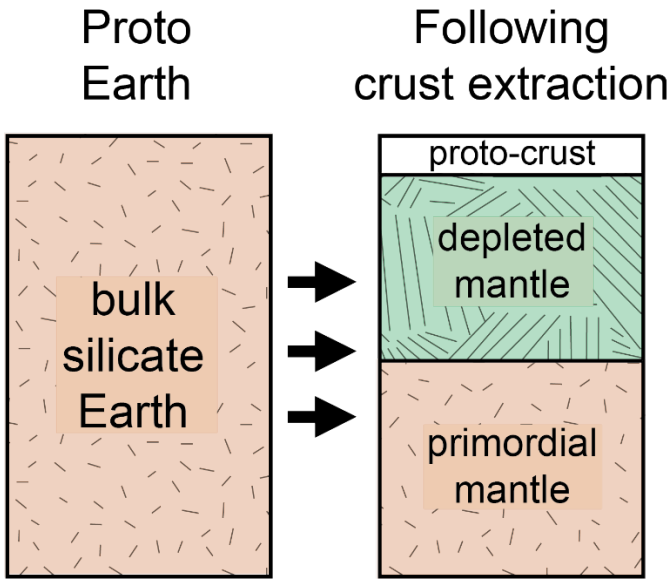

Supplementary Figure 10: During crust formation a portion of the bulk silicate Earth (BSE) is tapped and distributed among two reservoirs; a depleted mantle (DM) and a proto-crust (C). Given that only 30-50 % of whole mantle has been depleted to form the crust: $m_{DM} + m_C << m_{BSE}$, meaning a primordial mantle reservoir remains untapped.

748

749 The isotopic mass balance can be written as follows:

750 $$m_{BSE}[Mo]_{BSE}\,\delta_{BSE}^{98/95} = m_C[Mo]_C\,\delta_C^{98/95} + m_{DM}[Mo]_{DM}\delta_{DM}^{98/95} \quad (A)$$

751 Where m is the mass, [Mo] is the Mo concentration, and $\delta^{98/95}$ is the Mo isotope
752 composition (i.e. δ^{98}Mo) of the various reservoirs (BSE, DM and C).

753 The pure elemental mass balance is:

754 $$m_{BSE}[Mo]_{BSE} = m_C[Mo]_C + m_{DM}[Mo]_{DM} \quad (B)$$

where, the terms denote similar meanings as above.

Substituting for "$m_{AM}[Mo]_{BSE}$" in Eq. A by Eq. B, we have:

$$m_C[Mo]_C\,\delta_C^{98/95} = (m_C[Mo]_C + m_{DM}[Mo]_{DM})\,\delta_{BSE}^{98/95} - m_{DM}[Mo]_{DM}\,\delta_{DM}^{98/95}$$

$$m_C[Mo]_C\,(\delta_C^{98/95} - \delta_{BSE}^{98/95}) = m_{DM}[Mo]_{DM}(\delta_{BSE}^{98/95} - \delta_{DM}^{98/95})$$

$$\boldsymbol{m_C = \frac{m_{DM} \cdot [Mo]_{DM} \cdot (\delta_{BSE}^{98/95} - \delta_{DM}^{98/95})}{[Mo]_C \cdot (\delta_C^{98/95} - \delta_{BSE}^{98/95})}} \qquad \textbf{(C)}$$

This allows us to calculate the mass of crust generated assuming various amounts of depletion of the mantle reservoir (see Fig. 4).

The volume of this crust can then be calculated using the following:

$$V_{crust} = m_{crust} / \rho_{crust} \qquad (D)$$

where, V_c & ρ_c represent the volume and average density of the crust.

This volume is then easily comparable to the present volume of continental crust (PVCC) which is assumed to be 7.2 x10^9 km^3 [48]. The parameters used in mass balance calculations herein are presented in Table S5. Here we have investigated two scenarios to encompass the variability of δ^{98}Mo and [Mo] in Archean felsic rocks (granites or TTGs represent the felsic endmember; Fig. 4). Crustal volumes are then calculated for three different model Archean proto-crusts: a hypothetical purely felsic crust, Mafic crust-A (minimum based on a mafic crust) and Mafic crust-B (a likely Eoarchean crustal composition). The felsic crust TTG-crust is composed exclusively of granite or TTG rocks, while the Mafic crust-A and -B contain mafic rocks and TTGs felsic rocks in 50:50 and 75:25 proportions, respectively. Given the dominance of mafic lithologies within the Earth's early crust >3 Ga [49,50] it is reasonable to assume that the crust extracted prior to 3.5 Ga was more mafic than today.

Supplementary Text

Filtering for alteration and the composition of Archean komatiites

Due to their long residence in the crust the δ^{98}Mo of komatiites may have been modified by alteration or metamorphism due to the mobility of Mo in fluids [51,52]. Here we have used a plot of Mn/Fe^{2+} versus Al/Fe^{2+} to assess the extent of alteration in the komatiites (Fig. S1). This type of plot has been used previously to assess alteration in komatiites [1,2]. Given that Fe and Mn have similar chemical behaviour during magmatic differentiation; olivine generally has a similar Mn/Fe^{2+} as the initial melt, therefore addition or crystallisation of olivine will not significantly fractionate Mn/Fe^{2+}. Therefore, samples that plot perpendicular to the magmatic differentiation trend must have been affected by Fe or Mn mobilization and their δ^{98}Mo values may have been modified by secondary alteration after emplacement. For the data presented previously by Greber, et al. [3] the olivine-cumulates from the Weltevreden and Munro komatiites generally have more variable δ^{98}Mo than the spinifex-textured lavas at the same locations (Figs. 1 and S1); with the spinifex-texture samples falling close to the field defined by unaltered magmas undergoing magmatic differentiation. This may presumably be due to a higher proportion of easily altered olivine phenocrysts in the cumulate samples. However, there is no inherent reason why spinifex-texture samples should be less altered than cumulates, one of the spinifex-texture samples measured here has an extremely fractionated δ^{98}Mo (422-99 = +0.007‰) and has disrubed Mn/Fe^{2+}. Thus, exclusion for alteration needs to be done on a geochemical rather than rock type basis.

The averages presented here for the Weltevreden (−0.215 ±0.038‰) and Munro komatiites (−0.196 ±0.044‰; Table S3) have are identical within error to those calculated when including all of the Greber, et al. [3] data which are −0.206 ±0.071‰ (n = 7) for Weltevreden and −0.211 ±0.043‰ (n = 9) for Munro. Inlcusion of the previously excluded data also makes little difference to the average composition of Archean komatiites which

799 becomes −0.204 ±0.028‰ (n = 20) and remains resolvably sub-chondritic. In summary,
800 independent of the samples used and the rationale for excluding altered samples the
801 conclusion holds that Archean komatiites are sub-chondritic.
802
803 *The Baffin Island picrites and correlations with δ^{98}Mo*
804 The fact olivine accumulation controls the major element compositions of the Baffin Island
805 picrites is well established [12,53-56]. Here we show Mo concentrations of the Baffin Island
806 samples are strongly correlated with MgO, like many other trace elements (Fig. S3).
807 However, due to the incompatibility of Mo in olivine (D_{Mo} = 0.006 [30]), we would expect no
808 effect on δ^{98}Mo. Previous work by McCoy-West, et al. [12] showed the Fe and Zn isotope
809 compositions of individual olivines are as light as −0.8‰ for δ^{56}Fe and −0.3‰ for δ^{66}Zn ,
810 with the bulk rock compositions controlled by the accumulation of variable amounts of
811 olivine that is out of equilibrium with the melt (thus significant kinetic isotope fractionation
812 occurred). A strong covariation between δ^{98}Mo and δ^{66}Zn (Fig. S4) suggests these variations
813 are controlled by the same process, with correlations also seen versus trace element ratios or
814 elemental concentrations (Fig. S5). Presumably when this diffusional re-equilibration is
815 occurring for Fe and Zn, heavy Mo isotopes were also being preferentially removed from the
816 crystals and entering the melt (all things being equal heavy isotopes prefer the strongest
817 bonds [57]; i.e. lowest coordination number; see Table S7). Olivines that have then undergone
818 kinetic isotope exchange can then be extremely isotopically light. Variable amounts of these
819 unique olivines are then entrained in subsequent melts and due to the low concentration of
820 Mo in the melt can possibly affect the bulk rock composition.
821
822 From a mass balance standpoint this is hard to envisage due to the extreme
823 incompatibility of Mo in olivine. An alternate scenario is the Mo is hosted within chromite

or sulfide inclusions within the olivines. Leaching experiments were conducted on two samples (see Table S9) and the non-silicate (chromite or sulfide) fraction is resolvable isotopically lighter than the residual silicate trapped Mo, this non-silicate fraction also contains ~40 % of the Mo of the samples.

Ultimately, the exact nature of this correlation with respect to Mo isotopes is not particularly important for our purposes here. What is important is: 1) the strong linear trends versus a range of different trace element concentrations and ratios (Figs. S4 & S5) shows this is the result of linear addition (i.e. crystal accumulation) rather than magmatic differentiation (where parabolic curves would be expected); and 2) these correlations allow calculation of the composition of the Baffin Island parental melt (Table S2) which is identical within error to all of the other high temperature high degree partial melts measured from 3.5 Ga to the present (Table S3).

Estimates of the composition of Mid-ocean ridge basalts

The composition of the MORB mantle is a contentious issue in the Mo isotope scientific literature, with inconsistency between published results [22,23,46]. Initial work by Hibbert, et al. [58] processed ~1 g of handpicked glasses and obtain δ^{98}Mo values of ca. −0.15 to −0.25‰. A comprehensive study of MORB glasses by Bezard, et al. [22] found the average composition of normal MORB was −0.180 ±0.016‰ (n = 18; as in the main text all errors are 95% s.e.), with the five most depleted samples representative of depleted MORB, uncontaminated by recycled crustal sediments, being slightly sub-chondritic with a an average δ^{98}Mo of −0.206 ±0.021‰ (n = 5). These studies agree with the average composition of the least altered oceanic crust from ODP site 1256 reported as −0.20 ±0.06‰ (n = 5) [59]. In stark contrast, Liang, et al. [23] found an average MORB composition of δ^{98}Mo = +0.005 ±0.025‰ (n = 10). Here we have reanalysed one of the MORB samples presented in Liang, et al. [23] from the

North Atlantic Ridge (45N; provided by Kevin Burton in both cases) that had a reported composition of +0.03 ± 0.07‰. Our reanalysis produces an identical Mo concentration of 0.41 ppm, but a distinctly different δ^{98}Mo value of −0.159 ±0.056‰ (n = 2), which is in agreement with published values for enriched MORBs from the Mohs-Knipovich-Jan Mayen Ridge analysed by Bezard, et al. [22] which range from −0.08 to −0.15‰. This new analysis cast doubt over the MORB analyses presented in Liang, et al. [23]. Therefore, in this work we use the published MORB data presented in Bezard, et al. [22]. Emphasis here has been placed on the composition of the depleted MORB mantle because a range isotopic studies [60-62] have shown the majority of MORB samples are contaminated by recycled sedimentary material.

The composition of the endmembers used in crustal estimate calculations

Modern crustal values of δ^{98}Mo and [Mo] are probably not representative of the composition of the early proto-crust, hence here we have modelled a range of crust types using the best estimates of Archean compositions available. The composition of Archean crust can never be determined with certainty, because of the poor preservation of such old rocks [48]. Indirect approaches, however, suggest the crust was probably dominantly mafic in composition with a subordinate amount of felsic rocks e.g. [48-50,63,64]. Following this idea, we created 3 different compositions of Archean crust by mixing different amount of felsic and mafic rocks- *purely felsic*, *semi-mafic* and *dominantly-mafic*, which would fully encompass its compositional uncertainty. Clearly the first one is hypothetical, and the latter two are more representative of the Archean crust. For mass balance calculations, we needed two values- elemental, [Mo] and isotopic, δ^{98}Mo composition of Mo for the felsic and mafic counterparts (i.e., total four parameters):

1) Only [Mo] of Archean felsic rocks (TTGs and granites) are available [15] which we have used. For all the other parameters, we needed proxies.

874 2) The [Mo] of the basalt endmember (0.155) has been model based on partial melting of the
875 mantle by 30% (sitting in the middle of the Archean range; [19,20]) to produce a high Mg basalt
876 using well constrained D values; [17,30]. Due to the incompatible nature of Mo, varying the
877 degree of melting from 20 to 40% does not substantial change this value it from 0.23 to 0.12
878 ppm (Fig. S8).
879 3) We chose the δ^{98}Mo of average modern basalts (−0.10‰) to represent the mafic
880 endmember. The revised partial melting model shows that melting of a chondritic mantle
881 reservoir to form basalt would reproduce the global basalt average with ~15 % melting at
882 1300 °C. This ~0.05 ‰ offset is comparable to the natural offset observed between N-
883 MORB [22] and the accessible mantle herein. Melting at higher temperatures or greater degrees
884 of melting would result in a lighter melt. Changing of the composition of the basalt to
885 −0.12‰ (30% melt at 1400 °C) results in a difference in V_{PCC} of only 0.12 (for the 50:50
886 model at 30% mantle depletion), which is smaller than the already displayed error envelopes
887 based on varying endmember composition (see Fig. 4).
888 4) Archean felsic rocks are dominated by TTGs with rare granites (see [65] for a review). TTGs
889 are chemically evolved rocks (SiO_2 >65%) like granites, but they are primarily characterized
890 by higher Na/K values than true granites. For our purpose, it is important to see what the
891 likely difference in δ^{98}Mo between Archean TTGs and modern granites. The elemental
892 concentration of Mo in TTGs and modern and Archean granites are plotted in Figure S7.
893 Phanerozoic granites (Av. Mo = 0.90 ppm) have significantly higher [Mo] than Archean
894 TTGs (Av Mo = 0.28 ppm). Presumably because granites are the result of the multiple
895 episodes of reworking. Therefore, in Figure 4 we present two endmember models, a granite
896 model which provides minimum values of crustal volume and uses the δ^{98}Mo of modern
897 granites (+0.16‰) and a TTG model which represents the most realistic estimate based on
898 the available information of the volumes of early crust. Given that TTGs have lower Mo

concentrations than granites it is sensible to assume their δ^{98}Mo will also be less evolved. Here we have taken the simplest approach (i.e. two step formation of TTGs) and taken the average of global basalts and granites to estimate the δ^{98}Mo of TTG felsic component (+0.03‰).

There is no *a priori* reason to assume that partial melting processes were different in the Archean than they are today. Therefore, we do not expect significant uncertainties in the crustal volume presented in this study due to the lack of exact match between our chosen proxies for Archean crust and the real Archean crust.

The effect of partial melting on Mo isotopes

Two major factors, redox and co-ordination, will control the fractionation of Mo stable isotopes during partial melting e.g. [57]. Due to the oxidised nature of the terrestrial upper mantle (≈FMQ), in partial melts of this mantle, Mo predominantly occurs as tetrahedral coordinated Mo^{6+} (MoO_4^{2-}) [32,34]. Furthermore, given Mo^{6+} is significantly more incompatible than Mo^{4+} [30] melting products will have higher $Mo^{6+}/\sum Mo$ than their residue, and hence will be heavier. Co-ordination is a subordinate effect but will also result in an isotopically heavy melt, with Mo in pyroxene (octahedral; [33] and olivine having higher coordination than in the melt, with heavy isotopes preferentially moving to sites with the lowest coordination number [57]. The generation of isotopically heavy melts is consistent with the fact average global basalt (δ^{98}Mo = −0.10 ± 0.04‰; [16]), are isotopically heavier than the bulk accessible mantle we observe today (δ^{98}Mo = −0.20 ± 0.01‰; see Table S3). Because Mo is highly incompatible during mantle melting D_{Mo} = 0.006-0.008 [17,30], it will be quantitatively extracted into the melt except at low degrees of melting (see Fig. S8).

Here we have constructed a non-modal batch melting to show the fractionation of Mo isotopes during partial melting based upon the general principles outlined in Sossi and

O'Neill [31]. At high degrees of melting as observed in Archean komatiites and the Baffin Island picrites (20-40 % melting), they will remain essential unfractionated from their source region due to the complete removal of Mo from their residue. The corollary is that any Mo remaining in the residual mantle after partial melting is isotopically lighter. At smaller degrees of melting or more reduced conditions the $\Delta^{98}Mo_{melt\text{-}residue}$ can be larger (see Fig. 3).

Alternative estimates of the composition of the bulk silicate Earth

In the main text we have assumed the Mo isotope composition of the bulk silicate Earth (BSE) is the same as the chondritic meteorites Earth accreted from ($\delta^{98}Mo = -0.154 \pm 0.013$‰; [23,24]). Here we investigate the effects of alternate scenarios on the volume of crust extraction required in the early Earth: 1) the Mo isotope composition of BSE was modified during core formation; or 2) the composition of the BSE is the same as the bulk silicate Moon.

Modification during core formation (Model 2): The near quantitative removal of Mo to the metallic core means the metallic phase is unlikely to be fractionated from bulk chondrites, as is observed in iron meteorites [24]. However, this sequestration of Mo may have been associated with a small but resolvable isotopic fractionation of the silicate portion of the planet of up to 0.3‰ [24].

When extrapolating to temperatures more closely approximating core formation (>2000 °C [66]) initial metal-silicate equilibration experiments [67] suggested a resolvable $\Delta^{98}Mo_{metal\text{-}silicate}$ of −0.052‰ at 2500 °C, but subsequent work which incorporates the effect of Mo valance state [68] suggests a significantly reduced $\Delta^{98}Mo_{metal\text{-}silicate}$ of as little as −0.008‰ (assuming reduced conditions with $Mo^{6+}/\sum Mo = 0.1$). This parameterization requires accurate knowledge of both the temperature and oxygen fugacity at the time of core formation, neither of which we know with certainty. However, we can make an educated estimate on the maximum effect of core formation. Core formation is expected to occur between 2000 °C and 3000 °C [66,69-71]

and requires highly reduced conditions initially [66,72]. A reasonable upper estimate of the maximum effect of core formation could impart is $\Delta_{98\text{Mometal-silicate}} = -0.012$‰ (assuming T = 2000 °C; $Mo^{6+}/\sum Mo = 0.1$), meaning that if the mantle is indeed isotopically heavier it will still be within error of the composition of chondrites. Crustal volume estimates based on an isotopically heavier BSE following core formation ($\delta^{98}Mo = -0.142$‰) are presented in Figure S6 (c-d). These estimates are higher (3.4-5.3 times PVCC) but not drastically different than the modelling assuming a chondritic BSE.

Composition similar to bulk silicate Moon (Model 3): We also explored the effect of a BSE composition based on the Earth-Moon equilibration as done by Willbold and Elliott [46]. This idea is based on assuming the BSE and Moon were once isotopically equilibrated as has been shown for several lithophile elements [73,74]. Using analyses of lunar samples ($\delta^{98}Mo = -0.050 \pm 0.033$‰; [24]), and assuming subsequent late accretion of 1% chondritic material results in a $\delta^{98}Mo$ of −0.078‰. By using this value for the BSE and then undertaking mass balance modelling to investigate the volume of crust, generates unrealistically large volumes of crust (Fig. S6e-f). Namely, using TTG felsic materials for mafic crust-A (50:50 mafic-felsic rocks) and a depleted mantle comprising 30% of the mantle would require 14 times the PVCC. This value is even higher for the mafic crust-B (75:25 mafic-felsic rocks). Requiring >10 times the PVCC is highly unrealistic, considering the recycling rates and present extent of crustal volume. Therefore, for Mo it is extremely unlikely that the BSE was ever fully equilibrated with the bulk silicate Moon.

The effect of the lower crust

On the modern Earth the continental crust has a well-developed lower crust [48,63,64]. Estimates of the composition of the continental crust from molybdenites, granites and arc-related basalts are consistent with a super-chondritic $\delta^{98}Mo$ from +0.05 to +0.30‰ [16,75,76]. These

975 archives are focused on the upper continental crust (arc basalts are a record of juvenile
976 continental crust), but do not consider the effect of possible compositional variations in the
977 lower crust. However, given the extreme incompatibility of Mo during mantle melting D_{Mo} =
978 0.006-0.008 [17,30], Mo essentially becomes concentrated in the upper crust rather than any
979 lower crustal cumulates. An additional complication would be the presence of residual
980 sulfides, that due to its chalcophile behaviour will preferentially incorporate Mo. However,
981 given on the modern Earth most continental crust is predominantly formed in subduction-like
982 environments sulfide-saturation will generally be delayed (due to higher fO_2, and water
983 contents), and therefore Mo will remain in the melt phase and removed to the upper crust.
984 The composition and makeup of the Archean crust was not identical to modern crust
985 [48,63,64]. Therefore, whether the Archean crust has a well-defined lower crust similar to today
986 or not is unknown. Instead, studies infer that the whole Archean crust was dominantly mafic
987 and may have contained subordinate amount of granitoids [49,50,63]. We have considered this
988 factor while carrying out the mass balance modelling by using 3 different crustal
989 compositions: (1) purely felsic (100% granitoids); (2) semi-mafic (Mafic crust-A;
990 combination of mafic-felsic in 50:50); and (3) dominantly-mafic (Mafic crust-B; with a
991 mafic-felsic ratio of 75:25). The mafic component of the latter two crustal types is
992 approximated from the Mo isotope composition of global average of basalts (juvenile melt).
993 Now, TTGs form when these basalts get metamorphosed and partially melted at amphibolite
994 or eclogite facies e.g. [77,78]. Therefore, we should expect a depleted residual mass in the lower
995 crust complementing the TTG composition. But, this depleted lower crust is extremely
996 unlikely to remain preserved in the crust, due to the geodynamic setting where Hadean to
997 early Archean TTGs are inferred to have formed (i.e. a stagnant-lid regime: either when the
998 meta-basalts drip back into the mantle (delamination) or during the mantle lid overturn events
999 that recycle the pre-existing crust back to the mantle [65,78-80]). The crucial point is, the

1000 preserved crustal profile is largely devoid of residues formed after TTG extraction. Therefore,
1001 the crust is dominated by juvenile, melt-undepleted (meta-)basalts and granitoids. As stated
1002 above, our existing mass balance calculations consider both these components of the Archean
1003 crust as realistically as possible. Furthermore, even if some fraction of this TTG-depleted
1004 residual mass remains in the crust, it is likely to be of granulite to eclogite grade- where rutile
1005 exists [77]. It has been shown that in such cases, rutile should dominate the Mo-budget [15,81,82].
1006 Mo-concentration within such eclogitic rutile can vary within 2-7 ppm [82] and thermodynamic
1007 phase equilibria modelling suggests that the Archean meta-basalts would have contained not
1008 more than ~0.5 volume % of rutile [83]. In that case, the net Mo concentration will not deviate
1009 much from that of average basalt, which we have already considered for the mafic component
1010 of our model crustal types. This further attest that the crustal volume range bracketed by
1011 semi-mafic and dominantly-mafic crustal types potentially accounts for the variations due to
1012 any depleted lower crustal rocks.
1013

References

1 Hibbert, K. E. J., Williams, H. M., Kerr, A. C. & Puchtel, I. S. Iron isotopes in ancient and modern komatiites: Evidence in support of an oxidised mantle from Archean to present. *Earth and Planetary Science Letters* **321–322**, 198-207, doi:http://dx.doi.org/10.1016/j.epsl.2012.01.011 (2012).

2 Dauphas, N., Teng, F.-Z. & Arndt, N. T. Magnesium and iron isotopes in 2.7 Ga Alexo komatiites: Mantle signatures, no evidence for Soret diffusion, and identification of diffusive transport in zoned olivine. *Geochimica et Cosmochimica Acta* **74**, 3274-3291, doi:https://doi.org/10.1016/j.gca.2010.02.031 (2010).

3 Greber, N. D., Puchtel, I. S., Nägler, T. F. & Mezger, K. Komatiites constrain molybdenum isotope composition of the Earth's mantle. *Earth and Planetary Science Letters* **421**, 129-138, doi:https://doi.org/10.1016/j.epsl.2015.03.051 (2015).

4 DePaolo, D. J., Linn, A. M. & Schubert, G. The continental crustal age distribution: Methods of determining mantle separation ages from Sm-Nd isotopic data and application to the southwestern United States. *Journal of Geophysical Research: Solid Earth* **96**, 2071-2088, doi:10.1029/90jb02219 (1991).

5 Puchtel, I. S., Humayun, M., Campbell, A. J., Sproule, R. A. & Lesher, C. M. Platinum group element geochemistry of komatiites from the Alexo and Pyke Hill areas, Ontario, Canada 11Associate editor: R. J. Walker. *Geochimica et Cosmochimica Acta* **68**, 1361-1383, doi:https://doi.org/10.1016/j.gca.2003.09.013 (2004).

6 Puchtel, I. S. *et al.* Insights into early Earth from Barberton komatiites: Evidence from lithophile isotope and trace element systematics. *Geochimica et Cosmochimica Acta* **108**, 63-90, doi:https://doi.org/10.1016/j.gca.2013.01.016 (2013).

7 Starkey, N. A. *et al.* Helium isotopes in early Iceland plume picrites: Constraints on the composition of high 3He/4He mantle. *Earth and Planetary Science Letters* **277**, 91-100, doi:https://doi.org/10.1016/j.epsl.2008.10.007 (2009).

8 Sossi, P. A. *et al.* Petrogenesis and Geochemistry of Archean Komatiites. *Journal of Petrology* **57**, 147-184, doi:10.1093/petrology/egw004 (2016).

9 Kerr, A. C. La Isla de Gorgona, Colombia: A petrological enigma? *Lithos* **84**, 77-101, doi:http://dx.doi.org/10.1016/j.lithos.2005.02.006 (2005).

10 Jacobsen, S. B. Isotopic and chemical constraints on mantle-crust evolution. *Geochimica et Cosmochimica Acta* **52**, 1341-1350, doi:https://doi.org/10.1016/0016-7037(88)90205-0 (1988).

11 Jacobsen, S. B. & Wasserburg, G. J. The mean age of mantle and crustal reservoirs. *Journal of Geophysical Research: Solid Earth* **84**, 7411-7427, doi:doi:10.1029/JB084iB13p07411 (1979).

12 McCoy-West, A. J., Godfrey Fitton, J., Pons, M.-L., Inglis, E. C. & Williams, H. M. The Fe and Zn isotope composition of deep mantle source regions: Insights from Baffin Island picrites. *Geochimica et Cosmochimica Acta* **238**, 542-562, doi:https://doi.org/10.1016/j.gca.2018.07.021 (2018).

13 DePaolo, D. J. Crustal growth and mantle evolution: inferences from models of element transport and Nd and Sr isotopes. *Geochimica et Cosmochimica Acta* **44**, 1185-1196, doi:https://doi.org/10.1016/0016-7037(80)90072-1 (1980).

14 O'Nions, R. K., Evensen, N. M. & Hamilton, P. J. Geochemical modeling of mantle differentiation and crustal growth. *Journal of Geophysical Research: Solid Earth* **84**, 6091-6101, doi:doi:10.1029/JB084iB11p06091 (1979).

15 Greaney, A. T. *et al.* Geochemistry of molybdenum in the continental crust. *Geochimica et Cosmochimica Acta* **238**, 36-54, doi:https://doi.org/10.1016/j.gca.2018.06.039 (2018).

16 Yang, J. *et al.* The molybdenum isotopic compositions of I-, S- and A-type granitic suites. *Geochimica et Cosmochimica Acta* **205**, 168-186, doi:https://doi.org/10.1016/j.gca.2017.01.027 (2017).

17 Wang, Z. & Becker, H. Molybdenum partitioning behavior and content in the depleted mantle: Insights from Balmuccia and Baldissero mantle tectonites (Ivrea Zone, Italian Alps). *Chemical Geology* **499**, 138-150, doi:https://doi.org/10.1016/j.chemgeo.2018.09.023 (2018).

18 Palme, H. & O'Neill, H. S. C. in *Treatise on Geochemistry (Second Edition)* (eds Heinrich D. Holland & Karl K. Turekian) 1-39 (Elsevier, 2014).

19 Herzberg, C., Condie, K. & Korenaga, J. Thermal history of the Earth and its petrological expression. *Earth and Planetary Science Letters* **292**, 79-88, doi:https://doi.org/10.1016/j.epsl.2010.01.022 (2010).

20 Keller, C. B. & Schoene, B. Statistical geochemistry reveals disruption in secular lithospheric evolution about 2.5 Gyr ago. *Nature* **485**, 490, doi:10.1038/nature11024 https://www.nature.com/articles/nature11024#supplementary-information (2012).

21 Isoplot 3.71 v. 3.71 (Berkeley Geochronology Centre, 2008).

22 Bezard, R., Fischer-Gödde, M., Hamelin, C., Brennecka, G. A. & Kleine, T. The effects of magmatic processes and crustal recycling on the molybdenum stable isotopic composition of Mid-Ocean Ridge

Basalts. *Earth and Planetary Science Letters* **453**, 171-181, doi:http://dx.doi.org/10.1016/j.epsl.2016.07.056 (2016).
23 Liang, Y.-H. *et al.* Molybdenum isotope fractionation in the mantle. *Geochimica et Cosmochimica Acta* **199**, 91-111, doi:https://doi.org/10.1016/j.gca.2016.11.023 (2017).
24 Burkhardt, C., Hin, R. C., Kleine, T. & Bourdon, B. Evidence for Mo isotope fractionation in the solar nebula and during planetary differentiation. *Earth and Planetary Science Letters* **391**, 201-211, doi:http://dx.doi.org/10.1016/j.epsl.2014.01.037 (2014).
25 Yoder, C. F. in *Global Earth Physics: A Handbook of Physical Constants* Vol. AGU Reference Shelf (ed T. J. Ahrens) pp. 1–31 (American Geophysical Union,, 1995).
26 McDonough, W. F. in *Treatise on Geochemistry (First Edition)* Vol. 2 (eds Heinrich D. Holland & Karl K. Turekian) 547-568 (Elsevier, 2003).
27 Salters, V. J. M. & Stracke, A. Composition of the depleted mantle. *Geochemistry, Geophysics, Geosystems* **5**, doi:doi:10.1029/2003GC000597 (2004).
28 Rudnick, R. L. & Gao, S. in *Treatise on Geochemistry (Second Edition)* (eds Heinrich D. Holland & Karl K. Turekian) 1-51 (Elsevier, 2014).
29 Walter, M. J. in *Treatise of Geochemistry* Vol. 2.08 (ed R. W. Carlson) 363-394 (Elsevier, 2003).
30 Leitzke, F. P. *et al.* Redox dependent behaviour of molybdenum during magmatic processes in the terrestrial and lunar mantle: Implications for the Mo/W of the bulk silicate Moon. *Earth and Planetary Science Letters* **474**, 503-515, doi:https://doi.org/10.1016/j.epsl.2017.07.009 (2017).
31 Sossi, P. A. & O'Neill, H. S. C. The effect of bonding environment on iron isotope fractionation between minerals at high temperature. *Geochimica et Cosmochimica Acta* **196**, 121-143, doi:https://doi.org/10.1016/j.gca.2016.09.017 (2017).
32 O'Neill, H. S. C. & Eggins, S. M. The effect of melt composition on trace element partitioning: an experimental investigation of the activity coefficients of FeO, NiO, CoO, MoO2 and MoO3 in silicate melts. *Chemical Geology* **186**, 151-181, doi:http://dx.doi.org/10.1016/S0009-2541(01)00414-4 (2002).
33 Adam, J. & Green, T. Trace element partitioning between mica- and amphibole-bearing garnet lherzolite and hydrous basanitic melt: 1. Experimental results and the investigation of controls on partitioning behaviour. *Contributions to Mineralogy and Petrology* **152**, 1-17, doi:10.1007/s00410-006-0085-4 (2006).
34 Farges, F. o., Siewert, R., Brown, J. G. E., Guesdon, A. & Morin, G. Structural environments around molybdenum in silicate glasses and melts. I. Influence of composition and oxygen fugacity on the local structure of molybdenum. *The Canadian Mineralogist* **44**, 731-753, doi:10.2113/gscanmin.44.3.731 (2006).
35 Starkey, N. A. *Evolution of the Earth's mantle-crust-atmosphere system from the trace element and isotope geochemistry of the plume-mantle reservoir* PhD thesis, Ph.D. thesis, University of Edinburgh, (2009).
36 Sossi, P. A., Nebel, O., O'Neill, H. S. C. & Moynier, F. Zinc isotope composition of the Earth and its behaviour during planetary accretion. *Chemical Geology* **477**, 73-84, doi:https://doi.org/10.1016/j.chemgeo.2017.12.006 (2018).
37 Rudge, J. F., Reynolds, B. C. & Bourdon, B. The double spike toolbox. *Chemical Geology* **265**, 420-431, doi:http://dx.doi.org/10.1016/j.chemgeo.2009.05.010 (2009).
38 Willbold, M. *et al.* High-Precision Mass-Dependent Molybdenum Isotope Variations in Magmatic Rocks Determined by Double-Spike MC-ICP-MS. *Geostandards and Geoanalytical Research* **40**, 389-403, doi:10.1111/j.1751-908X.2015.00388.x (2016).
39 Greber, N. D., Siebert, C., Nägler, T. F. & Pettke, T. δ98/95Mo values and Molybdenum Concentration Data for NIST SRM 610, 612 and 3134: Towards a Common Protocol for Reporting Mo Data. *Geostandards and Geoanalytical Research* **36**, 291-300, doi:10.1111/j.1751-908X.2012.00160.x (2012).
40 Goldberg, T. *et al.* Resolution of inter-laboratory discrepancies in Mo isotope data: an intercalibration. *Journal of Analytical Atomic Spectrometry* **28**, 724-735, doi:10.1039/c3ja30375f (2013).
41 Creech, J. B. & Paul, B. IsoSpike: Improved Double-Spike Inversion Software. *Geostandards and Geoanalytical Research* **39**, 7-15, doi:10.1111/j.1751-908X.2014.00276.x (2015).
42 Paton, C., Hellstrom, J., Paul, B., Woodhead, J. & Hergt, J. Iolite: Freeware for the visualisation and processing of mass spectrometric data. *Journal of Analytical Atomic Spectrometry* **26**, 2508-2518 (2011).
43 Neely, R. A. *et al.* Molybdenum isotope behaviour in groundwaters and terrestrial hydrothermal systems, Iceland. *Earth and Planetary Science Letters* **486**, 108-118, doi:10.1016/j.eps1.2017.11.053 (2018).

44 Zhao, P.-P. *et al.* Molybdenum Mass Fractions and Isotopic Compositions of International Geological Reference Materials. *Geostandards and Geoanalytical Research* **40**, 217-226, doi:10.1111/j.1751-908X.2015.00373.x (2015).
45 Yang, J. *et al.* Absence of molybdenum isotope fractionation during magmatic differentiation at Hekla volcano, Iceland. *Geochimica et Cosmochimica Acta* **162**, 126-136, doi:http://dx.doi.org/10.1016/j.gca.2015.04.011 (2015).
46 Willbold, M. & Elliott, T. Molybdenum isotope variations in magmatic rocks. *Chemical Geology* **449**, 253-268, doi:https://doi.org/10.1016/j.chemgeo.2016.12.011 (2017).
47 Hofmann, A. W. Mantle geochemistry: the message from oceanic volcanism. *Nature* **385**, 219, doi:10.1038/385219a0 (1997).
48 Cawood, P. A., Hawkesworth, C. J. & Dhuime, B. The continental record and the generation of continental crust. *GSA Bulletin* **125**, 14-32, doi:10.1130/B30722.1 (2013).
49 Dhuime, B., Wuestefeld, A. & Hawkesworth, C. J. Emergence of modern continental crust about 3 billion years ago. *Nature Geoscience* **8**, 552, doi:10.1038/ngeo2466 https://www.nature.com/articles/ngeo2466#supplementary-information (2015).
50 Tang, M., Chen, K. & Rudnick, R. L. Archean upper crust transition from mafic to felsic marks the onset of plate tectonics. *Science* **351**, 372-375, doi:10.1126/science.aad5513 (2016).
51 Bali, E., Keppler, H. & Audetat, A. The mobility of W and Mo in subduction zone fluids and the Mo–W–Th–U systematics of island arc magmas. *Earth and Planetary Science Letters* **351–352**, 195-207, doi:http://dx.doi.org/10.1016/j.epsl.2012.07.032 (2012).
52 Keppler, H. & Wyllie, P. J. Partitioning of Cu, Sn, Mo, W, U, and Th between melt and aqueous fluid in the systems haplogranite-H2O−HCl and haplogranite-H2O−HF. *Contributions to Mineralogy and Petrology* **109**, 139-150, doi:10.1007/bf00306474 (1991).
53 Clarke, D. B. Tertiary basalts of Baffin Bay: Possible primary magma from the mantle. *Contributions to Mineralogy and Petrology* **25**, 203-224, doi:10.1007/bf00371131 (1970).
54 Francis, D. The Baffin Bay lavas and the value of picrites as analogues of primary magmas. *Contributions to Mineralogy and Petrology* **89**, 144-154, doi:10.1007/BF00379449 (1985).
55 Larsen, L. M. & Pedersen, A. K. Processes in high-Mg, high-T magmas: Evidence from olivine, chromite and glass in Palaeogene picrites from West Greenland. *Journal of Petrology* **41**, 1071-1098, doi:10.1093/petrology/41.7.1071 (2000).
56 Starkey, N. A., Fitton, J. G., Stuart, F. M. & Larsen, L. M. Melt inclusions in olivines from early Iceland plume picrites support high 3He/4He in both enriched and depleted mantle. *Chemical Geology* **306–307**, 54-62, doi:https://doi.org/10.1016/j.chemgeo.2012.02.022 (2012).
57 Schauble, E. A. Applying Stable Isotope Fractionation Theory to New Systems. *Reviews in Mineralogy and Geochemistry* **55**, 65-111 (2004).
58 Hibbert, K., Freymuth, H., Willbold, M. & Elliott, T. Mass-dependent molybdenum isotopes in mid-ocean ridge basalts: A new mantle reference. *American Geophysical Union Fall Meeting* **San Francisco, California**, Abstract V52A-04 (2013).
59 Freymuth, H., Vils, F., Willbold, M., Taylor, R. N. & Elliott, T. Molybdenum mobility and isotopic fractionation during subduction at the Mariana arc. *Earth and Planetary Science Letters* **432**, 176-186, doi:http://dx.doi.org/10.1016/j.epsl.2015.10.006 (2015).
60 Nielsen, S. G. *et al.* Barium isotope evidence for pervasive sediment recycling in the upper mantle. *Science Advances* **4**, doi:10.1126/sciadv.aas8675 (2018).
61 Andersen, M. B. *et al.* The terrestrial uranium isotope cycle. *Nature* **517**, 356, doi:10.1038/nature14062 https://www.nature.com/articles/nature14062#supplementary-information (2015).
62 Rehkamper, M. & Hofmann, A. W. Recycled ocean crust and sediment in Indian Ocean MORB. *Earth and Planetary Science Letters* **147**, 93-106, doi:https://doi.org/10.1016/S0012-821X(97)00009-5 (1997).
63 Kamber, B. S., Whitehouse, M. J., Bolhar, R. & Moorbath, S. Volcanic resurfacing and the early terrestrial crust: Zircon U–Pb and REE constraints from the Isua Greenstone Belt, southern West Greenland. *Earth and Planetary Science Letters* **240**, 276-290, doi:https://doi.org/10.1016/j.epsl.2005.09.037 (2005).
64 Cawood, P. A. *et al.* Geological archive of the onset of plate tectonics. *Philosophical Transactions of the Royal Society A: Mathematical, Physical and Engineering Sciences* **376**, 20170405, doi:10.1098/rsta.2017.0405 (2018).
65 Moyen, J.-F. & Laurent, O. Archaean tectonic systems: A view from igneous rocks. *Lithos* **302-303**, 99-125, doi:https://doi.org/10.1016/j.lithos.2017.11.038 (2018).
66 Wade, J. & Wood, B. J. Core formation and the oxidation state of the Earth. *Earth and Planetary Science Letters* **236**, 78-95, doi:https://doi.org/10.1016/j.epsl.2005.05.017 (2005).

67 Hin, R. C., Burkhardt, C., Schmidt, M. W., Bourdon, B. & Kleine, T. Experimental evidence for Mo isotope fractionation between metal and silicate liquids. *Earth and Planetary Science Letters* **379**, 38-48, doi:http://dx.doi.org/10.1016/j.epsl.2013.08.003 (2013).
68 Hin, R. C., Burnham, A. D., Gianolio, D., Walter, M. J. & Elliott, T. Molybdenum isotope fractionation between Mo4+ and Mo6+ in silicate liquid and metallic Mo. *Chemical Geology* **504**, 177-189, doi:https://doi.org/10.1016/j.chemgeo.2018.11.014 (2019).
69 Siebert, J., Corgne, A. & Ryerson, F. J. Systematics of metal–silicate partitioning for many siderophile elements applied to Earth's core formation. *Geochimica et Cosmochimica Acta* **75**, 1451-1489, doi:https://doi.org/10.1016/j.gca.2010.12.013 (2011).
70 Righter, K., Pando, K. M., Danielson, L. & Lee, C.-T. Partitioning of Mo, P and other siderophile elements (Cu, Ga, Sn, Ni, Co, Cr, Mn, V, and W) between metal and silicate melt as a function of temperature and silicate melt composition. *Earth and Planetary Science Letters* **291**, 1-9, doi:http://dx.doi.org/10.1016/j.epsl.2009.12.018 (2010).
71 Ballhaus, C. *et al.* The U/Pb ratio of the Earth's mantle—A signature of late volatile addition. *Earth and Planetary Science Letters* **362**, 237-245, doi:https://doi.org/10.1016/j.epsl.2012.11.049 (2013).
72 Wade, J., Wood, B. J. & Tuff, J. Metal–silicate partitioning of Mo and W at high pressures and temperatures: Evidence for late accretion of sulphur to the Earth. *Geochimica et Cosmochimica Acta* **85**, 58-74, doi:http://dx.doi.org/10.1016/j.gca.2012.01.010 (2012).
73 Armytage, R. M. G., Georg, R. B., Williams, H. M. & Halliday, A. N. Silicon isotopes in lunar rocks: Implications for the Moon's formation and the early history of the Earth. *Geochimica et Cosmochimica Acta* **77**, 504-514, doi:https://doi.org/10.1016/j.gca.2011.10.032 (2012).
74 Young, E. D. *et al.* Oxygen isotopic evidence for vigorous mixing during the Moon-forming giant impact. *Science* **351**, 493, doi:10.1126/science.aad0525 (2016).
75 Voegelin, A. R., Pettke, T., Greber, N. D., von Niederhäusern, B. & Nägler, T. F. Magma differentiation fractionates Mo isotope ratios: Evidence from the Kos Plateau Tuff (Aegean Arc). *Lithos* **190–191**, 440-448, doi:http://dx.doi.org/10.1016/j.lithos.2013.12.016 (2014).
76 Greber, N. D., Pettke, T. & Nägler, T. F. Magmatic–hydrothermal molybdenum isotope fractionation and its relevance to the igneous crustal signature. *Lithos* **190-191**, 104-110, doi:https://doi.org/10.1016/j.lithos.2013.11.006 (2014).
77 Moyen, J.-F. & Martin, H. Forty years of TTG research. *Lithos* **148**, 312-336, doi:http://dx.doi.org/10.1016/j.lithos.2012.06.010 (2012).
78 Johnson, T. E., Brown, M., Gardiner, N. J., Kirkland, C. L. & Smithies, R. H. Earth's first stable continents did not form by subduction. *Nature* **543**, 239, doi:10.1038/nature21383 https://www.nature.com/articles/nature21383#supplementary-information (2017).
79 Sizova, E., Gerya, T., Stüwe, K. & Brown, M. Generation of felsic crust in the Archean: A geodynamic modeling perspective. *Precambrian Research* **271**, 198-224, doi:https://doi.org/10.1016/j.precamres.2015.10.005 (2015).
80 Rozel, A. B., Golabek, G. J., Jain, C., Tackley, P. J. & Gerya, T. Continental crust formation on early Earth controlled by intrusive magmatism. *Nature* **545**, 332, doi:10.1038/nature22042 (2017).
81 Fitton, J. G. Coupled molybdenum and niobium depletion in continental basalts. *Earth and Planetary Science Letters* **136**, 715-721, doi:https://doi.org/10.1016/0012-821X(95)00171-8 (1995).
82 Zack, T., Kronz, A., Foley, S. F. & Rivers, T. Trace element abundances in rutiles from eclogites and associated garnet mica schists. *Chemical Geology* **184**, 97-122, doi:https://doi.org/10.1016/S0009-2541(01)00357-6 (2002).
83 Johnson, T. E., Brown, M., Kaus, B. J. P. & VanTongeren, J. A. Delamination and recycling of Archaean crust caused by gravitational instabilities. *Nature Geoscience* **7**, 47, doi:10.1038/ngeo2019 https://www.nature.com/articles/ngeo2019#supplementary-information (2013).